ARR No. 4B10

NATIONAL ADVISORY COMMITTEE FOR AERONAUTICS

WARTIME REPORT

ORIGINALLY ISSUED

February 1944 as
Advance Restricted Report 4B10

EFFECTS OF PROPELLER OPERATION AND ANGLE OF YAW ON THE DISTRIBUTION OF THE LOAD ON THE HORIZONTAL TAIL SURFACE OF A TYPICAL PURSUIT AIRPLANE

By Harold H. Sweberg and Richard C. Dingeldein

Langley Memorial Aeronautical Laboratory
Langley Field, Va.

NACA

WASHINGTON

NATIONAL ADVISORY COMMITTEE FOR AERONAUTICS

ADVANCE RESTRICTED REPORT

EFFECTS OF PROPELLER OPERATION AND ANGLE OF YAW ON THE DISTRIBUTION OF THE LOAD ON THE HORIZONTAL TAIL SURFACE OF A TYPICAL PURSUIT AIRPLANE

By Harold H. Sweberg and Richard C. Dingeldein

SUMMARY

Measurements were made in the NACA full-scale tunnel of the pressure distribution over the horizontal tail surface of a typical pursuit airplane in order to determine the effects of propeller operation and angle of yaw on the tail load distribution. Most of the tests were made with the propeller operating to simulate climb conditions, high-speed dives, and pull-ups to various normal accelerations for angles of yaw ranging from 10° to -10°. Measurements were also made of the distributions of downwash angle and dynamic pressure in front of the horizontal tail and the results have been correlated with the results of the pressure-distribution tests.

From the results of the tests, it appears that the most severe asymmetrical loading condition for the horizontal tail will occur during a pull-up from high speed when appreciable yaw may be developed. It is shown that the angle of yaw is the most important factor contributing to the magnitude of the tail-load asymmetry. The magnitude of the tail-load asymmetry for unaccelerated, unyawed flight at low speeds and high propeller torque coefficients was sufficiently small to be of little importance. The difference in the normal-force coefficients on the two sides of the horizontal tail surface was dependent only on the angle of yaw and the power condition and was essentially independent of the elevator setting or the magnitude of the tail load.

INTRODUCTION

Numerous structural failures of the tail surfaces of military aircraft have recently occurred, especially in

dives. One of the factors contributing to these failures is the asymmetric tail loading that occurs as a result of slipstream rotation and airplane yaw. It has been suspected that under certain conditions this asymmetric loading may cause bending moments on the tail which are in excess of those calculated by current design criterions. Tests were accordingly conducted in the NACA full-scale tunnel to determine the distribution of the load on the horizontal tail surface of a typical pursuit airplane under conditions simulating actual flight.

The tests included pressure measurements over the horizontal tail of the P-40K airplane and air-flow surveys in front of the tail for various angles of attack and angles of yaw. Most of the tests were made with the propeller operating at coefficients simulating rated power at an altitude of 10,000 feet for conditions of both steady and accelerated flight. In addition, some tests were run with the propeller removed to determine the effects of propeller operation. A few force tests were made to determine the variation of the lift with the angle of attack of the airplane.

The data presented in this report are quantitative for the P-40K airplane only; it is believed, however, that the results should provide a basis for a qualitative evaluation of the effects of power and of yaw on the tail-load asymmetry of reasonably similar airplanes. It should also be pointed out that, inasmuch as the tests were conducted at low speeds and with relatively low tail-surface loads, the effects of Mach number and of elastic deformation are not included in these results.

SYMBOLS

C_L airplane lift coefficient $(L/q_o S_w)$

C_N tail normal-force coefficient $(N/q_o S_t)$

ΔC_N difference between normal-force coefficients on left and right tail surfaces $(C_{N_L} - C_{N_R})$

c_n section normal-force coefficient $\left(\frac{\text{tail section normal force}}{q_o c_t}\right)$

Q_c	torque coefficient $\left(Q/\rho V_o^2 D^3\right)$
T_c	thrust coefficient $\left(\frac{\text{effective thrust}}{\rho V_o^2 D^2}\right)$
L	airplane lift
N	tail normal force
ΔN	difference in normal force on left and right tail surfaces $(N_L - N_R)$
n	airplane load factor, also propeller rotational speed
Q	propeller torque
P	pressure coefficient $\left(\Delta p/q_o\right)$
Δp	difference in local static pressure between upper and lower surfaces of tail
S_w	wing area
S_t	horizontal-tail area, not including fuselage
c_t	tail chord
D	propeller diameter
x	lateral distance along tail span measured from fuselage center line
q	dynamic pressure $\left(\frac{1}{2}\rho V^2\right)$
V	velocity
V/nD	propeller advance-diameter ratio
ρ	mass density of air
H	altitude, feet
α_T	angle of attack of thrust axis relative to free-stream direction, degrees
ψ	angle of yaw, degrees; positive with left wing forward

ϵ	downwash angle, degrees
$\Delta\epsilon$	difference between downwash angles over right and left tail surfaces $(\epsilon_R - \epsilon_L)$
i_t	angle of stabilizer setting with respect to thrust axis, degrees; positive with trailing edge down
δ	control-surface deflection, degrees; positive with trailing edge down
β	propeller blade angle at 0.75 radius, degrees

Subscripts:

o	free stream
t	horizontal tail surface
e	elevator
R	right side of horizontal tail
L	left side of horizontal tail
av	average

METHODS AND TESTS

The tests were conducted on the Curtiss P-40K, which is a low-wing pursuit airplane weighing 7740 pounds and equipped with a V-1710-F4R Allison engine rated at 1000 horsepower at an altitude of 10,800 feet. A three-view drawing showing the principal dimensions of the airplane is given in figure 1 and a photograph of the airplane mounted in the NACA full-scale tunnel is given as figure 2.

For the pressure measurements, flush-type orifices were installed in the upper and lower surfaces of the horizontal tail at 12 chordwise stations symmetrically located across the span. The location and identification of the orifices are given in table I and in figure 3. The cellular construction of the tail surfaces prevented the installation of pressure orifices very

near the leading edge. In order to overcome this deficiency a method based on theoretical calculations, which will be described under "Results and Discussion," was used to obtain the pressure peaks at the leading edge of the tail.

The air-flow surveys consisted of downwash-angle and dynamic-pressure measurements in a vertical plane located 3.8 feet (average tail chord) ahead of the leading edge of the root section of the horizontal tail. A rake of 14 steel survey tubes, each capable of measuring the local downwash and sidewash angles and the local dynamic pressure, was used for these measurements. The horizontal tail surface was in place for all the air-flow measurements.

All the tests were made at a tunnel airspeed of approximately 85 miles per hour. The propeller blade angle, for the power-on tests, was set at 35° at the 0.75 radius and was held constant. By choosing this particular blade angle, it was possible to reproduce in the tunnel the torque coefficient of the constant-speed propeller exactly for all lift coefficients and, in addition, very nearly to reproduce the thrust coefficient. Figure 4 shows the variation of blade angle and V/nD with lift coefficient and figure 5 shows the variation of Q_c and T_c with lift coefficient for the constant-speed propeller and for the propeller operating at constant blade angle. The variation of lift coefficient with angle of attack of the airplane with the propeller removed and with the propeller operating at rated power at an altitude of 10,000 feet is shown in figure 6.

A summary of the complete test program is given in table II. The tests with the propeller operating were made to simulate both level-flight conditions and pull-ups to various normal accelerations of the airplane. The maneuvers that were reproduced are given in the last column of table II in terms of airplane load factor. For the level-flight conditions ($n = 1.00$), the elevator angles were set for trim according to the results of unpublished flight-test data. For the accelerated-flight conditions, tests were made at two or three elevator angles in order to bracket the probable elevator deflection required to pull up to the normal acceleration listed. The yaw-angle range ($\psi = \pm 10°$) was chosen to bracket the

maximum angle of yaw likely to be encountered in the maneuvers being considered.

RESULTS AND DISCUSSION

Chordwise pressure distributions.- The pressure measurements were first plotted along the various chord lines of the horizontal tail surface to obtain the chordwise distribution of the tail load. Inasmuch as there were no orifices very near the leading edge of the tail, the following method was used to estimate the leading-edge pressure peaks: The theory of reference 1 shows that for a symmetrical airfoil a point on the chordwise distribution curve bears the same relationship to any other point regardless of the lift supplied by the section, provided that the surface has not stalled. The leading-edge pressure peaks were estimated by a direct comparison of that portion of the measured distribution near the leading edge with the corresponding part of the theoretical curve. For all these tests, the elevator settings were sufficiently small that the effect of deflecting the elevator on the leading-edge pressure peaks could be neglected (reference 2).

A few typical chordwise pressure distributions over the tail of the P-40K airplane are shown in the isometric charts of figures 7 to 13. Included in each of these figures are the corresponding distributions of section normal-force coefficient across the tail span that were obtained by integrating the chordwise pressure distributions. The effects of the slipstream rotation and the angle of yaw on the distribution of the tail load are included in these figures. Comparison of figures 7 and 9 shows the effect of the slipstream rotation on the tail load distribution at a low value of C_L and Q_c; the effect of the slipstream rotation at a high value of C_L and Q_c may be obtained by comparing figures 8 and 10. At a low value of Q_c, which corresponds to a high-speed or dive condition, the effect of propeller operation on the distribution of section normal-force coefficient is small. At the high value of Q_c (low-speed climb), propeller operation resulted in a large increase in the normal-force coefficient on the left side of the tail and a correspondingly large

decrease in the normal-force coefficient on the right side of the tail. The effect of angle of yaw on the tail load distribution is shown in figures 10 to 13 for a lift coefficient of 0.820 with rated power applied. The asymmetries in the tail load distribution due to yaw, even at $\psi = 5^\circ$, are very large.

Spanwise distributions of normal-force coefficient.- Curves showing the spanwise distribution of section normal-force coefficient are given in figures 14 to 20. Span load distributions, with the propeller removed, at three angles of yaw ($\psi = 0^\circ$, 5°, and 10°) are shown in figures 14 to 16. These tests were made to determine the effects of yaw on the distribution of tail load and to serve as a basis for determining the effects of propeller operation. With the propeller removed and $\psi = 0^\circ$, the load on the left side of the tail was higher than the load on the right side of the tail. This asymmetry is essentially independent of the angle of attack of the airplane and is probably due to differences in the airplane on the two sides of the plane of symmetry and also to a side-flow component of the wind-tunnel air stream.

Span load distributions with the propeller operating at rated power at an altitude of 10,000 feet are shown in figures 17 to 20 for four angles of yaw ($\psi = 0^\circ$, 5°, 10°, and -10°) and include lift coefficients bracketing an airplane velocity range from 150 to 550 miles per hour. The elevator angles for these tests were set for trim at the corresponding lift coefficient for unaccelerated flight. The small variation with the airplane lift coefficient of the elevator angle required for trim is due to the low degree of longitudinal stability of the airplane. It is very evident from the figures that large changes in the distribution of normal-force coefficient along the tail span result from both propeller operation and angle of yaw.

The distribution of the load on the horizontal tail surface under conditions simulating a typical pull-up from high speed, when $C_L = 0.820$ and $n = 9.0$ ($V = 450$ mph), is given in figure 21. The results are given for two elevator settings ($\delta_e = -1.0^\circ$ and -5.0°) inasmuch as the exact elevator setting for the maneuver was not known. Although the magnitude of the tail load was changed by elevator deflection, the distribution of

the load across the tail span remained substantially the same. In general, the effects of propeller operation and yaw on the tail load distribution for this case are similar to the effects measured for the unaccelerated-flight conditions.

In order to estimate the magnitude of the tail loads and the asymmetry in the tail load resulting from propeller operation and yaw, average values for the tail normal-force coefficient have been computed for each side of the horizontal tail surface by integrating spanwise distributions of $c_n c_t$. The complete results of these calculations, which are based on free-stream dynamic pressure, are given in table III. It is pointed out that the maximum bending moment on the tail for a particular condition does not depend on the magnitude of ΔC_N in all cases but depends on the distribution of the load across the horizontal-tail span.

Air-flow measurements.- Measurements were made of the downwash angles and the dynamic pressures in front of the tail in order to correlate the results of the tail pressure measurements with the geometric pattern of the air flow in front of the tail. The tail surfaces were in place for the air-flow measurements but, inasmuch as this report is primarily concerned with differences in the tail loads and the downwash angles on both sides of the plane of symmetry of the airplane, it is believed that the inclination of the air stream in front of the tail due to the presence of the tail will have little effect on the conclusions drawn from the results of these measurements.

A few typical examples showing the variation of downwash angle and dynamic pressure across the tail span together with the corresponding spanwise distribution of normal-force coefficient are shown in figures 22 to 28. The survey patterns for each of these conditions are shown in figures 29 to 35, which were plotted for the same test conditions as the chordwise pressure distributions shown in figures 7 to 13. The increase in downwash angle on the side of the tail behind the downgoing propeller blades and the corresponding decrease in the downwash on the side of the upgoing propeller blades are evident from examination of figures 29 to 35. Large changes in the downwash angles near the fuselage were measured when the airplane was yawed with

the propeller operating. Comparison of figures 25 and 28 shows the large increase in the downwash angle on the left side of the horizontal tail near the fuselage due to yawing the airplane to -10°. For positive angles of yaw, with the propeller operating, the downwash angles on the right side of the tail near the fuselage are decreased and the downwash angles near the outboard section of the right side of the tail are increased from the values obtained at zero yaw. (Compare figs. 25 to 27.)

Explanations of the combined effects of the slipstream and the yaw angle on the tail load distribution are very difficult owing to the complex nature of the slipstream, especially in yawed flight. Some sketches have been prepared (fig. 36) to show estimated slipstream patterns for the various yaw conditions. It is known that the mean path of the slipstream in yawed flight will lie somewhere between the direction of the relative wind and the longitudinal axis of the airplane. Studies of the span load distributions and the air-flow measurements showed that for a first approximation this angle may be taken as one-half the angle of yaw. The combined effects of power and yaw appear to be critically dependent on the direction in which the airplane is yawed. As the airplane is yawed in a positive direction (left wing forward), an increasingly greater percentage of the right side of the tail (which is blanketed by the fuselage) will be immersed in the air stream affected by the upgoing propeller blades and the combined effects of power and yaw will tend to decrease the asymmetry of the tail load. As the airplane is yawed in a negative direction, an increasingly greater percentage of the blanketed side of the tail will be immersed in the air stream affected by the downgoing propeller blades and the combined effects of power and yaw will tend to increase the asymmetry of the tail load.

In order to aid in correlating the air-flow surveys with the pressure-distribution measurements, calculations have been made to obtain the average downwash angle and the average dynamic-pressure ratio for each side of the tail. The values of $\left(q/q_o\right)_{av}$ have been weighted according to the spanwise variation of tail chord and the values of ϵ_{av} have been weighted according to the spanwise variation of tail chord and dynamic-pressure ratio by the formulas

$$\left(\frac{q}{q_o}\right)_{av} = \frac{2}{S_t}\int_0^{b_t/2} c_t \frac{q}{q_o}\, dx$$

$$\epsilon_{av} = \frac{2}{\left(\frac{q}{q_o}\right)_{av} S_t}\int_0^{b_t/2} \epsilon c_t \frac{q}{q_o}\, dx$$

The values of q/q_o and ϵ used for these calculations were taken at the intersection of the plane through the horizontal tail and the survey plane. The results for all the test conditions are given in table III together with the values of the average normal-force coefficients.

Curves have been plotted (fig. 37) that show the variations in the differences of average downwash over the right and left tail surfaces with angle of yaw for various torque coefficients. The slope of the curve of $\Delta\epsilon_{av}$ against ψ near zero yaw was about 0.8 for the propeller-removed condition. Propeller operation at various constant values of Q_c had little effect on this value. The difference in downwash on the two sides of the horizontal tail at zero yaw was about 6° greater with the propeller operating at $Q_c = 0.036$ than with the propeller removed.

An analysis has been made to correlate the measured downwash asymmetry with the asymmetry in normal-force coefficient. Points plotted in figure 38 show the variations of $\Delta C_{N_{av}}$ with $\Delta\epsilon_{av}$ for all the test conditions and a mean curve has been drawn through the test points. The values of $\Delta C_{N_{av}}$ given in figure 37 are based on local dynamic pressure in order that any asymmetries due to the differences in dynamic pressure on both sides of the horizontal tail may be eliminated. The slope of the curve of $\Delta C_{N_{av}}$ against $\Delta\epsilon_{av}$, at $\Delta\epsilon_{av} = 0°$, is about 0.02 per degree. This value is of the order of magnitude that may be expected for a twisted wing having a low aspect ratio and acting in a uniform stream.

Tail-load asymmetry.- Calculations have been made of the difference between the load on the right and the left sides of the horizontal tail surface for the various test conditions. The variation of tail-load asymmetry with angle of yaw is shown in figure 39 at three lift coefficients for the airplane with the propeller removed. Figure 40 shows the tail-load asymmetry as a function of angle of yaw for various steady-flight lift coefficients of the airplane with the propeller operating. The data of figures 39 and 40 have been replotted in figure 41 to show separately the effects of power and of yaw on the tail-load asymmetry. At $C_L = 0.066$ (V = 550 mph at an altitude of 10,000 ft) and $\psi = 10^\circ$, the difference in the load on the right and left surfaces due only to yaw was 1000 pounds. Propeller operation corresponding to steady flight at this lift coefficient resulted in a tail-load asymmetry of -650 pounds. The net tail-load asymmetry for this condition was therefore 350 pounds. At the same lift coefficient but $\psi = -10^\circ$, a net tail-load asymmetry of about -1400 pounds can be obtained by extrapolating the curve of figure 38 to $\psi = -10^\circ$. The combined effects of power and of yaw, for right-hand propeller operation, are therefore more severe when the airplane is yawed in a negative direction than when the airplane is yawed in a positive direction. The magnitude of the tail-load asymmetry at the high lift coefficients for unaccelerated flight was sufficiently small to be of little consequence.

The asymmetries in the tail load for various pull-up maneuvers are shown in figure 42. Inasmuch as the exact elevator deflections for the maneuvers were not known, the measurements were made for a range of elevator angle. The results show, however, that the asymmetry in the tail load is primarily dependent on the power condition and the angle of yaw and is essentially independent of the elevator setting or the magnitude of the tail load.

It appears that in actual flight the most important factor contributing to the magnitude of the tail-load asymmetry will be the angle of yaw or of sideslip developed. At high values of C_L or low airplane velocities the tail loads will be small and the effects of power or yaw on the tail-load asymmetry will be of little consequence. At high velocities when the tail loads may

assume considerable proportions, the effects of propeller operation on the tail-load asymmetry will be small inasmuch as the propeller torque and thrust coefficients will be very low. The asymmetry due to yaw at high velocities, however, may be considerable, especially during pull-up maneuvers when large angles of sideslip may be developed. The sideslip developed by an airplane during a high-speed pull-up is primarily due to the gyroscopic action of the propeller. As a typical example, during flight tests of the P-40 airplane (unpublished), the airplane yawed noticeably to the right in all pull-ups. Calculations showed that, when the propeller rotational speed was 1140 rpm, as in the cruising condition, a pitching velocity of 0.4 radian per second may result in a yawing moment of about 5000 foot-pounds, which could be offset by a steady angle of sideslip of approximately 10° at a velocity of 175 miles per hour.

SUMMARY OF RESULTS

The results of measurements made in the NACA full-scale tunnel on a typical pursuit airplane to determine the effects of propeller operation and angle of yaw on the tail load distribution showed the following:

1. Large differences between the average downwash angles on the two sides of the horizontal tail surfaces as a result of propeller operation and yaw were measured. At zero yaw, the difference between the average downwash angles on the two sides of the horizontal tail was about 6° greater with the propeller operating at a torque coefficient of 0.036 than with the propeller removed. The change in the difference between the average downwash angles on the two sides of the tail per degree change in angle of yaw was about 0.8 for the airplane with propeller removed.

2. The difference between the average normal-force coefficients on the two sides of the horizontal tail per degree difference in the average downwash angle was about 0.02.

3. The results of the tests showed that the most important factor contributing to the magnitude of the tail-load asymmetry will be the angle of yaw developed

during a pull-up at high speed and with single-rotating right-hand propellers will be most severe when the airplane yaws in a negative direction.

4. The net asymmetry of the tail load calculated for a typical high-speed dive (a speed of 550 mph) due to both propeller operation and yaw was -1400 pounds when the airplane was yawed in a negative direction (right wing forward) and was 350 pounds when the airplane was yawed in a positive direction.

5. The magnitude of the tail-load asymmetry for unaccelerated flight at high lift coefficients was sufficiently small to be unimportant.

6. The asymmetry in the tail load was essentially independent of the elevator setting or the magnitude of the tail load.

Langley Memorial Aeronautical Laboratory,
National Advisory Committee for Aeronautics,
Langley Field, Va.

REFERENCES

1. Jacobs, Eastman N., and Rhode, R. V.: Airfoil Section Characteristics as Applied to the Prediction of Air Forces and Their Distribution on Wings. Rep. No. 631, NACA, 1938.

2. Allen, H. Julian: Calculation of the Chordwise Load Distribution over Airfoil Sections with Plain, Split, or Serially Hinged Trailing-Edge Flaps. Rep. No. 634, NACA, 1938.

Table I.- Chordwise Location of Orifices on the P-40K Horizontal Tail, Inches Aft of Leading Edge.

Row / Orifice	1	2	3	4	5	6	7	8	9	10	11	12
1	3 1/2	3 1/2	3	2 3/4	2 1/4	2	2 1/4	2 1/2	3	3	3 1/2	4
2	7 1/2	7 1/2	5 1/2	6	5 1/4	5 1/4	5 1/4	5 1/2	6	5 1/2	7 1/2	7 1/2
3	11 1/4	12 1/2	11	12 1/2	9 1/2	11	10 3/4	10	12 1/2	11	12 1/2	11
4	14 1/4	17 1/2	15 3/4	19 1/2	14 1/2	15 1/4	15 1/2	14 1/2	19 1/2	15 3/4	17 1/2	14
5	18 3/4	22	20 1/4	25 3/4	22 1/4	24 1/4	24 1/2	22	25 3/4	20 1/4	21 3/4	18 1/2
6	21 3/4	25	25	29 3/4	28 1/2	32 1/2	32 3/4	29 1/4	29 3/4	25	25 1/4	21 3/4
7	24 1/4	28 3/4	28 1/2	32 3/4	32 1/4	36 1/4	36 1/4	32 3/4	32 1/2	28 1/4	28 3/4	24
8	3 1/2	32 1/4	32	38 1/2	36 1/2	40	40 1/4	36 1/2	38 1/2	32	32	4
9	7 1/2	36 3/4	36 1/2	43 1/2	40	43	43	39 1/2	43 1/4	36 1/4	36 1/2	7 1/2
10	11 1/4	3 1/2	41	47 3/4	44	48	46 1/2	43 3/4	47 1/2	41	3 1/2	11
11	14 1/4	7 1/2	3	50 1/2	48 3/4	2	2 1/4	48 1/2	50	3	7 1/2	14
12	18 3/4	12 1/2	5 1/2	2 3/4	52 1/2	5 1/4	5 1/4	52 1/2	3	5 1/2	12 1/2	18 1/2
13	21 3/4	17 1/2	11	6	55 1/4	11	10 3/4	55	6	11	17 1/2	21 3/4
14	24 1/4	22	15 3/4	12 1/2	2 1/4	15 1/4	15 1/2	2 1/2	12 1/2	15 3/4	21 3/4	24
15		25	20 1/4	19 1/2	5 1/4	24 1/4	24 1/2	5 1/2	19 1/2	20 1/4	25 1/4	
16		28 3/4	25	25 3/4	9 1/2	32 1/2	32 3/4	10	25 3/4	25	28 3/4	
17		32 1/4	28 1/2	29 3/4	14 1/2	36 1/4	36 1/4	14 1/2	29 3/4	28 1/4	32	
18		36 3/4	32	32 3/4	22 1/4	40	40 1/4	22	32 1/2	32	36 1/2	
19			36 1/2	38 1/2	28 1/2	43	43	29 1/4	38 1/2	36 1/4		
20			41	43 1/2	32 1/4	48	46 1/2	32 3/4	43 1/4	41		
21				47 3/4	36 1/2			36 1/2	47 1/2			
22				50 1/2	40			39 1/2	50			
23					44			43 3/4				
24					48 3/4			48 1/2				
25					52 1/2			52 1/2				
26					55 1/4			55				

Table II.- P-40K Test Program

Run	C_L	α_T, deg	ψ, deg	δ_e, deg	Propeller	V/nD	β, deg	n
1	0.066	-1.10	0	-0.4	off	—	—	—
2	.294	1.90	0	- .4		—	—	—
3	.820	8.70	0	-1.0		—	—	—
4	.066	-1.10	5	- .4		—	—	—
5	.294	1.90	5	- .4		—	—	—
6	.820	8.70	5	-1.0		—	—	—
7	.066	-1.10	10	- .4		—	—	—
8	.294	1.90	10	- .4		—	—	—
9	.820	8.70	10	-1.0	off	—	—	—
10	.066	-1.10	0	- .4	on	1.70	35	1.00
11	.150	- .30	0	- .4		1.56		1.00
12	.294	1.60	0	- .4		1.37		1.00
13	.294	1.60	0	- .4		1.56		1.96
14	.294	1.60	0	-5.0		1.56		1.96
15	.294	1.70	0	- .4		1.70		4.46
16	.294	1.70	0	-5.0		1.70		4.46
17	.820	7.40	0	-1.0		.99		1.00
18	.820	7.80	0	-1.0		1.37		2.79
19	.820	7.80	0	-5.0		1.37		2.79
20	.820	7.80	0	-10.0		1.37		2.79
21	.820	8.20	0	-1.0		1.65		9.02
22	.820	8.20	0	-5.0		1.65		9.02
23	.066	-1.10	5	- .4		1.70		1.00
24	.150	- .30	5	- .4		1.56		1.00
25	.294	1.60	5	- .4		1.37		1.00
26	.294	1.60	5	- .4		1.56		1.96
27	.294	1.60	5	-5.0		1.56		1.96
28	.294	1.70	5	- .4		1.70		4.46
29	.294	1.70	5	-5.0		1.70		4.46
30	.820	7.40	5	-1.0		.99		1.00
31	.820	7.80	5	-1.0		1.37		2.79
32	.820	7.80	5	-5.0		1.37		2.79
33	.820	8.20	5	-1.0		1.65		9.02
34	.820	8.20	5	-5.0		1.65		9.02
35	.066	-1.10	10	- .4		1.70		1.00
36	.150	- .30	10	- .4		1.56		1.00
37	.294	1.60	10	- .4		1.37		1.00
38	.294	1.60	10	- .4		1.56		1.96
39	.294	1.60	10	-5.0		1.56		1.96
40	.294	1.70	10	- .4		1.70		4.46
41	.294	1.70	10	-5.0		1.70		4.46
42	.820	7.40	10	-1.0		.99		1.00
43	.820	7.80	10	-1.0		1.37		2.79
44	.820	7.80	10	-5.0		1.37		2.79
45	.820	8.20	10	-1.0		1.65		9.02
46	.820	8.20	10	-5.0		1.65		9.02
47	.066	-1.10	-10	- .4		1.70		1.00
48	.150	- .30	-10	- .4		1.56		1.00
49	.294	1.60	-10	- .4		1.37		1.00
50	.294	1.60	-10	- .4		1.56		1.96
51	.294	1.70	-10	- .4		1.70		4.46
52	.820	7.40	-10	-1.0		.99		1.00
53	.820	7.80	-10	-1.0		1.37		2.79
54	.820	8.20	-10	-1.0	on	1.65	35	9.02

Table III. – P-40K Test Results

Run	C_N	C_{N_R}	C_{N_L}	ϵ_{av_R}, deg	ϵ_{av_L}, deg	$(\frac{q}{q_\infty})_{av_R}$	$(\frac{q}{q_\infty})_{av_L}$
1	−0.108	−0.131	−0.085	3.3	2.6	0.94	0.93
2	− .027	− .050	− .003	4.5	3.8	.96	.97
3	.130	.109	.150	8.0	7.7	.98	.94
4	− .072	− .120	− .023	5.3	1.4	.95	.97
5	− .020	− .077	.038	7.1	2.3	.95	.95
6	.137	.071	.203	10.8	5.6	.94	.96
7	− .070	− .133	− .008	8.1	−0.9	.95	.94
8	− .022	− .096	.053	9.1	0.4	.96	.97
9	.113	.034	.191	12.3	3.2	.91	.95
10	− .044	− .065	− .023	3.8	2.4	.97	.99
11	− .023	− .055	.009	4.9	2.6	.98	1.00
12	− .033	− .080	.014	7.7	2.9	1.08	1.03
13	− .035	− .067	− .003	6.1	3.7	1.01	.96
14	− .120	− .168	− .071	6.1	3.6	1.01	.96
15	.016	− .017	.049	5.3	3.0	1.00	.98
16	− .109	− .133	− .084	5.3	3.0	1.00	.98
17	.086	− .038	.209	12.8	6.1	1.45	1.18
18	.100	.041	.159	10.4	7.6	1.16	1.04
19	.022	− .037	.080	10.4	7.6	1.16	1.04
20	− .132	− .199	− .062	10.4	7.6	1.16	1.04
21	.114	.076	.152	10.9	8.3	1.07	.93
22	.013	− .036	.062	10.9	8.3	1.07	.93
23	− .072	− .115	− .029	4.6	0.2	.93	.99
24	− .064	− .113	− .014	4.7	0.1	.93	.99
25	− .035	− .090	.021	7.2	2.0	1.03	1.03
26	− .040	− .104	.025	7.2	1.7	.98	1.02
27	− .104	− .163	− .045	7.2	1.7	.98	1.02
28	− .037	− .097	.023	6.6	2.1	.95	.98
29	− .106	− .167	− .044	6.6	2.1	.95	.98
30	.032	− .079	.143	13.6	3.6	1.28	1.17
31	.070	− .015	.155	14.3	4.2	1.04	1.08
32	.018	− .071	.107	14.3	4.2	1.04	1.08
33	.071	− .011	.153	13.1	5.0	1.01	.98
34	.025	− .057	.107	13.1	5.0	1.01	.98
35	− .023	− .069	.014	6.4	−0.9	.94	.97
36	.019	− .012	.049	7.7	−0.4	.97	.98
37	.063	.030	.096	—	—	—	—
38	.046	.008	.084	8.7	0.6	.95	.97
39	− .089	− .154	− .023	8.7	0.6	.95	.97
40	.045	− .007	.096	8.9	0.8	.93	1.00
41	− .076	− .121	− .024	8.9	0.8	.93	1.00
42	.158	.110	.205	11.4	2.9	1.10	1.05
43	.131	.100	.201	11.3	4.0	1.00	.98
44	.080	.024	.136	11.3	4.0	1.00	.98
45	.129	.061	.196	12.3	3.7	.95	.98
46	.070	− .009	.148	12.3	3.7	.95	.98
47	− .089	− .057	− .121	1.8	5.9	.96	1.07
48	− .086	− .049	− .122	2.0	7.7	.98	1.10
49	− .079	− .032	− .125	3.3	8.0	1.10	1.15
50	− .051	− .003	− .099	2.0	10.1	1.02	1.07
51	− .063	− .010	− .095	2.6	8.7	.96	1.07
52	− .032	.064	− .127	5.1	7.9	1.31	1.33
53	.040	.128	− .049	7.9	13.3	1.07	1.09
54	.063	.142	− .016	6.7	13.5	1.00	1.00

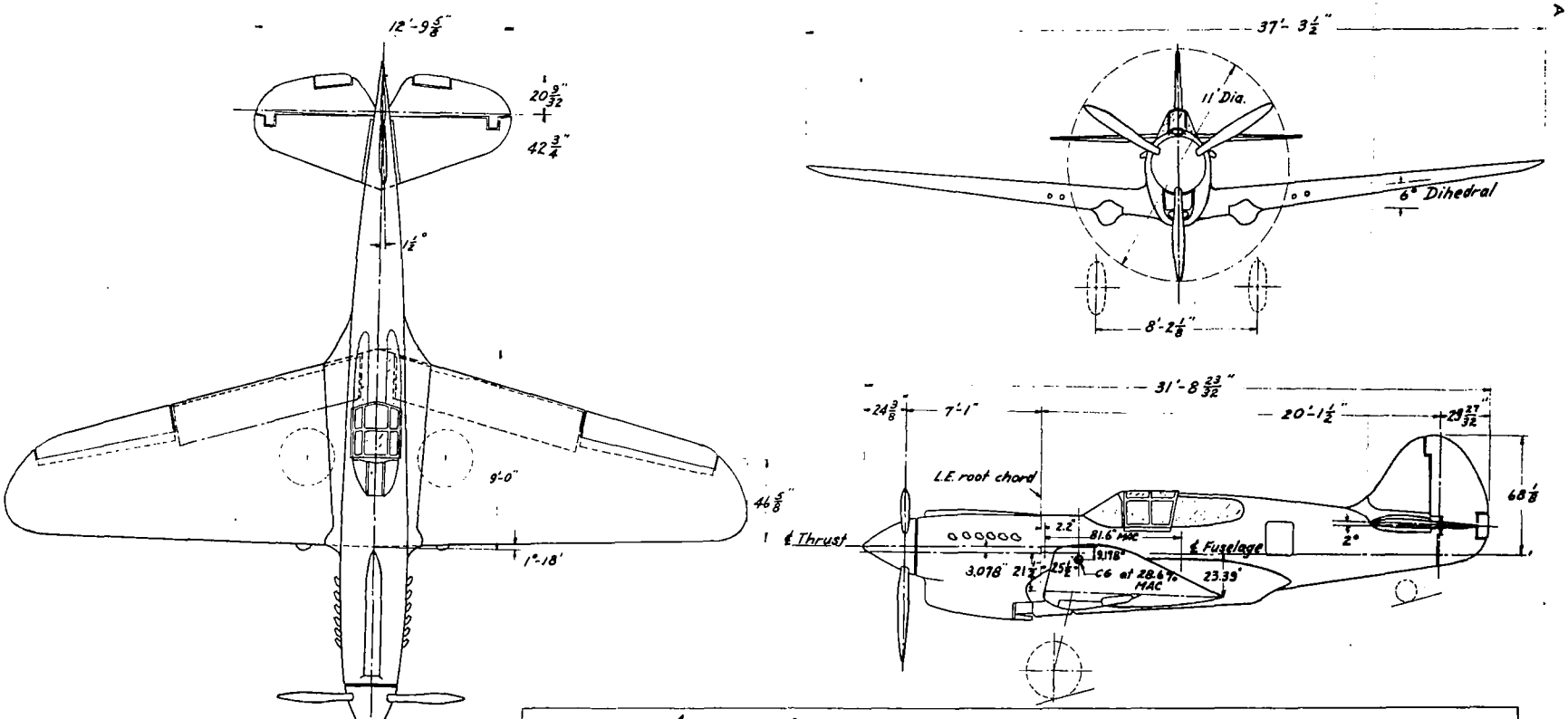

Areas, sq ft			
Wing, total	236	Engine	Allison V-1710-F4R
Stabilizer (incl. 3.56 sq ft of fuselage)	30.86	BHP normal rating - 1000 at 2600 rpm at 10,800 ft	
Elevator (incl. 3.8 sq ft balance, 1.68 sq ft tab)	17.44	Propeller gear ratio	2:1
Fin	9.18	Gross weight, design	7740 lb
Rudder (incl. 1.94 sq ft balance, 0.55 sq ft tab)	13.74		

Figure 1.-Three-view drawing of the P-40K airplane.

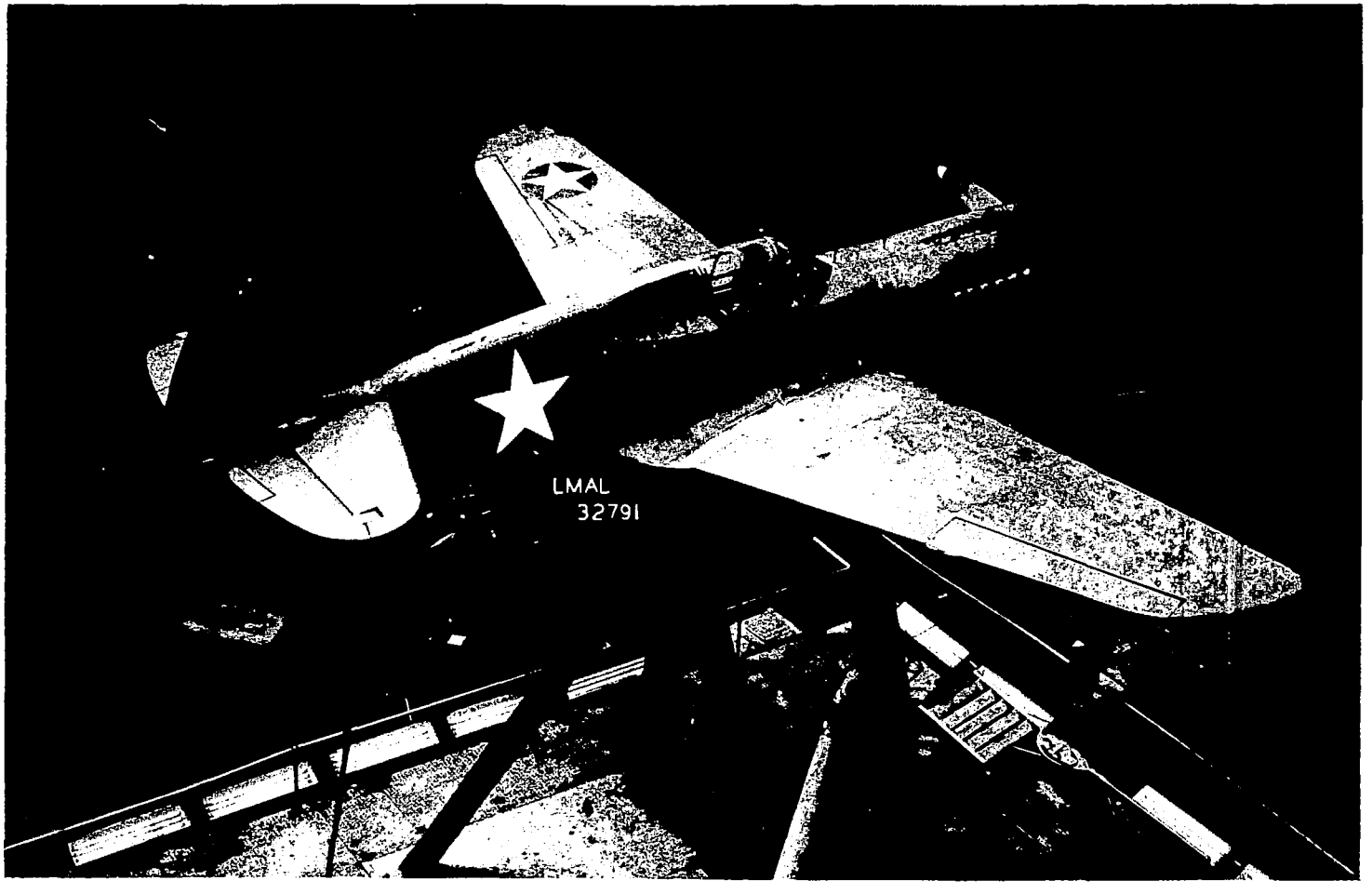

Figure 2 - The P-40K airplane mounted in the NACA full-scale tunnel.

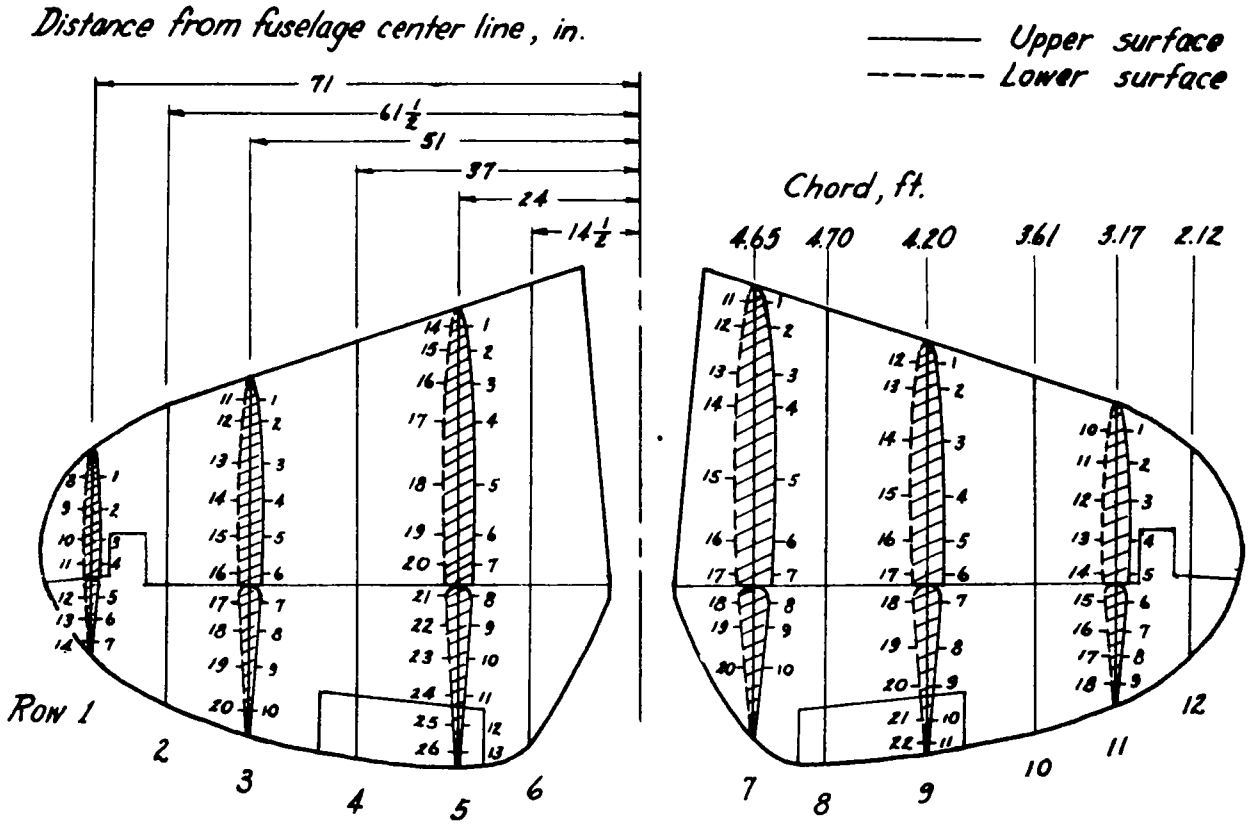

Figure 3.-Location and identification of orifices on the P-40K horizontal tail surface.

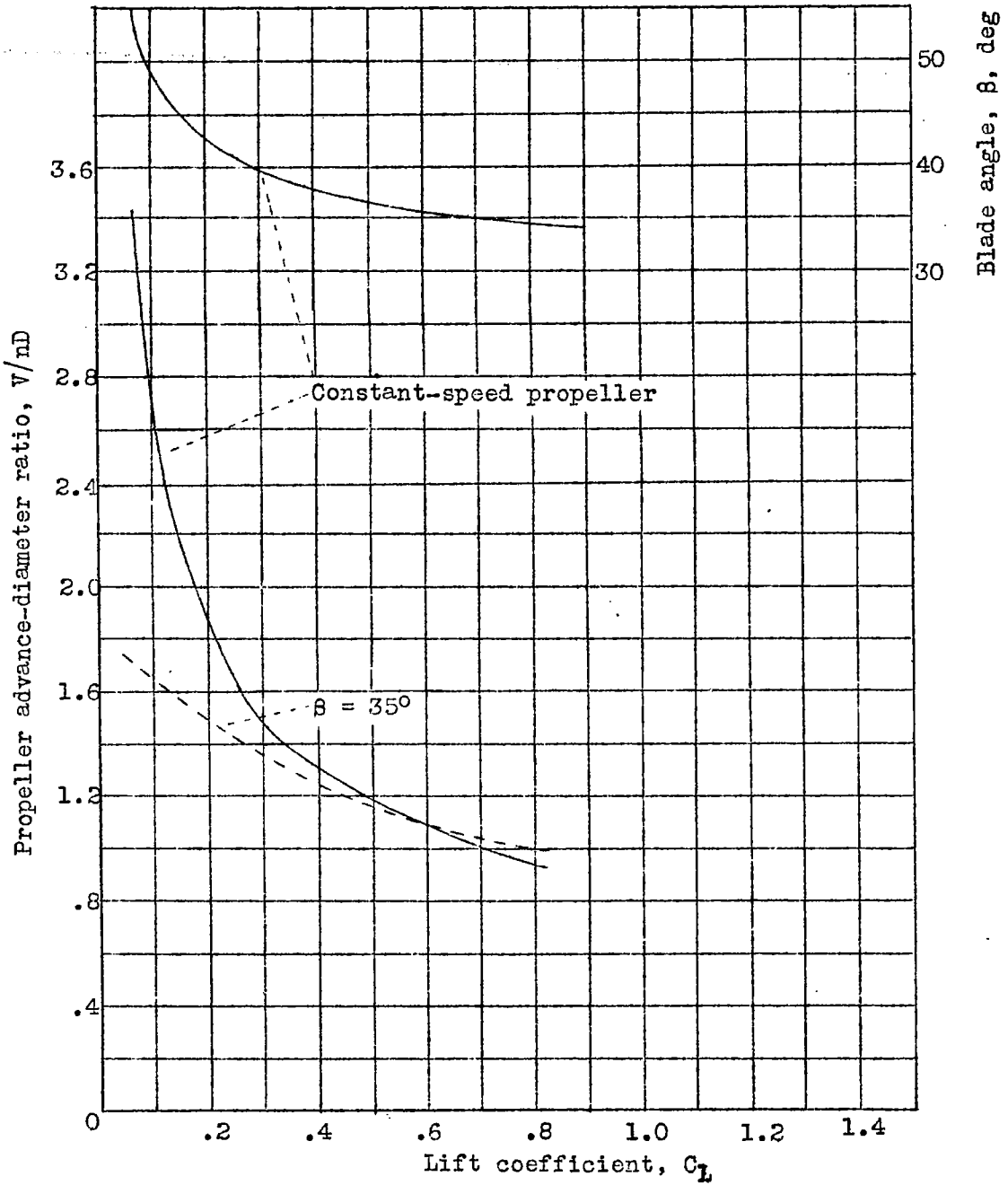

Figure 4.- Variation of β and V/nD with C_L for the constant-speed propeller and the propeller operating at constant blade angle. Rated power at 10,000 feet altitude.

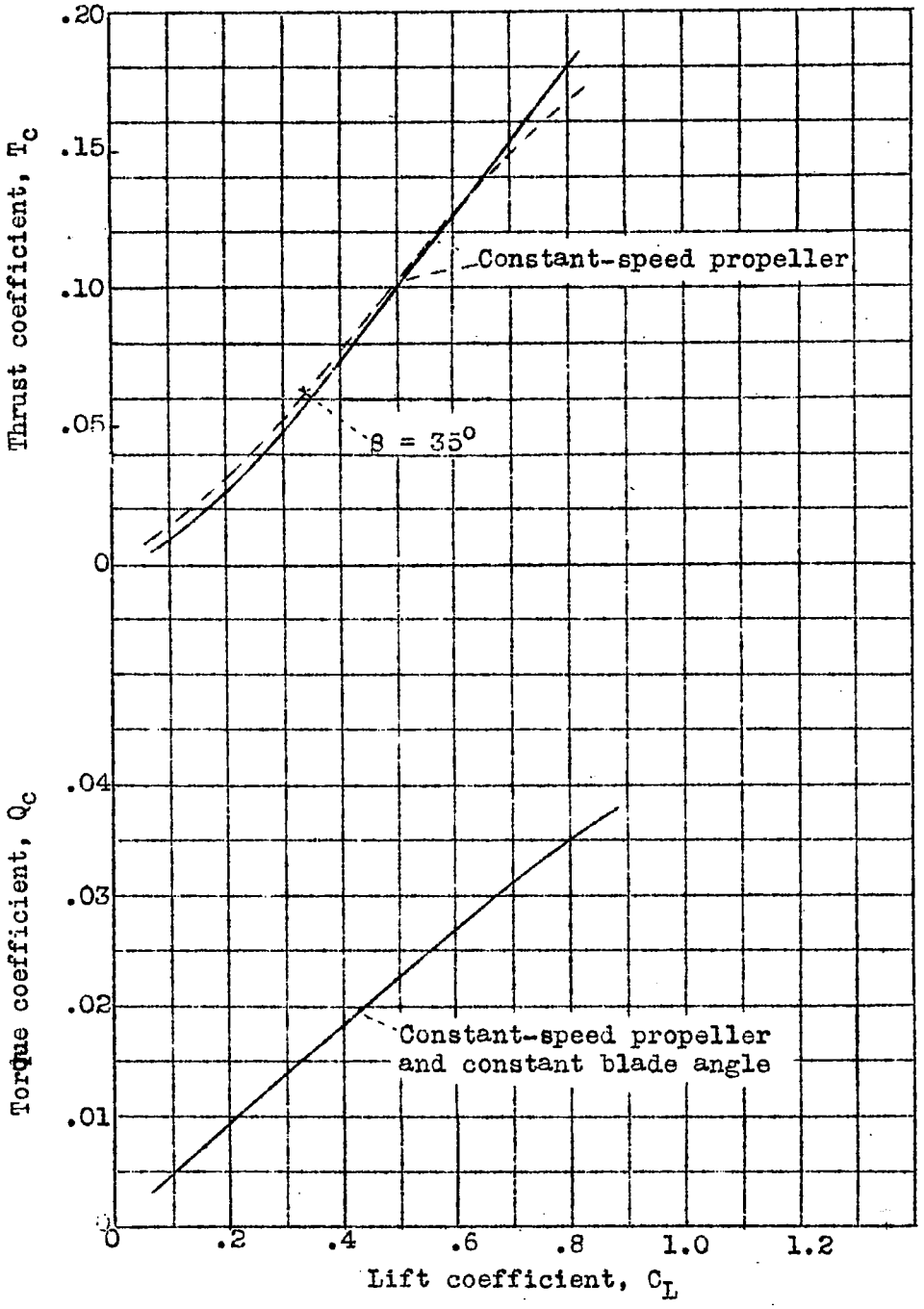

Figure 5.- Variation of T_c and Q_c with C_L for the constant-speed propeller and the propeller operating at constant blade angle. Rated power at 10,000 feet altitude.

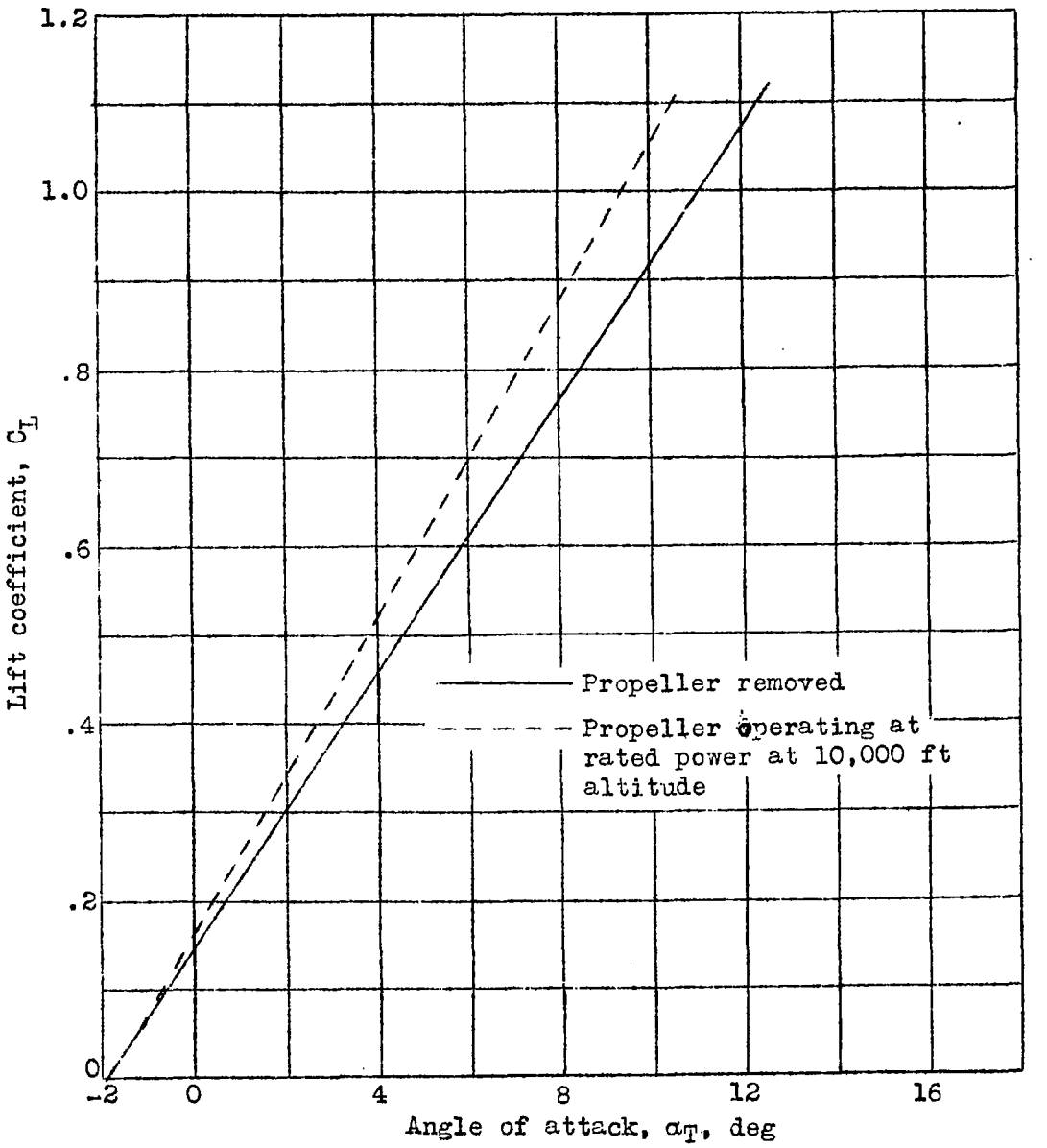

Figure 6.- Lift curves for the P-40K airplane with the propeller removed and operating at rated power at 10,000 feet altitude. Flaps retracted; i_t, 2.0°; δ_e, -0.4°.

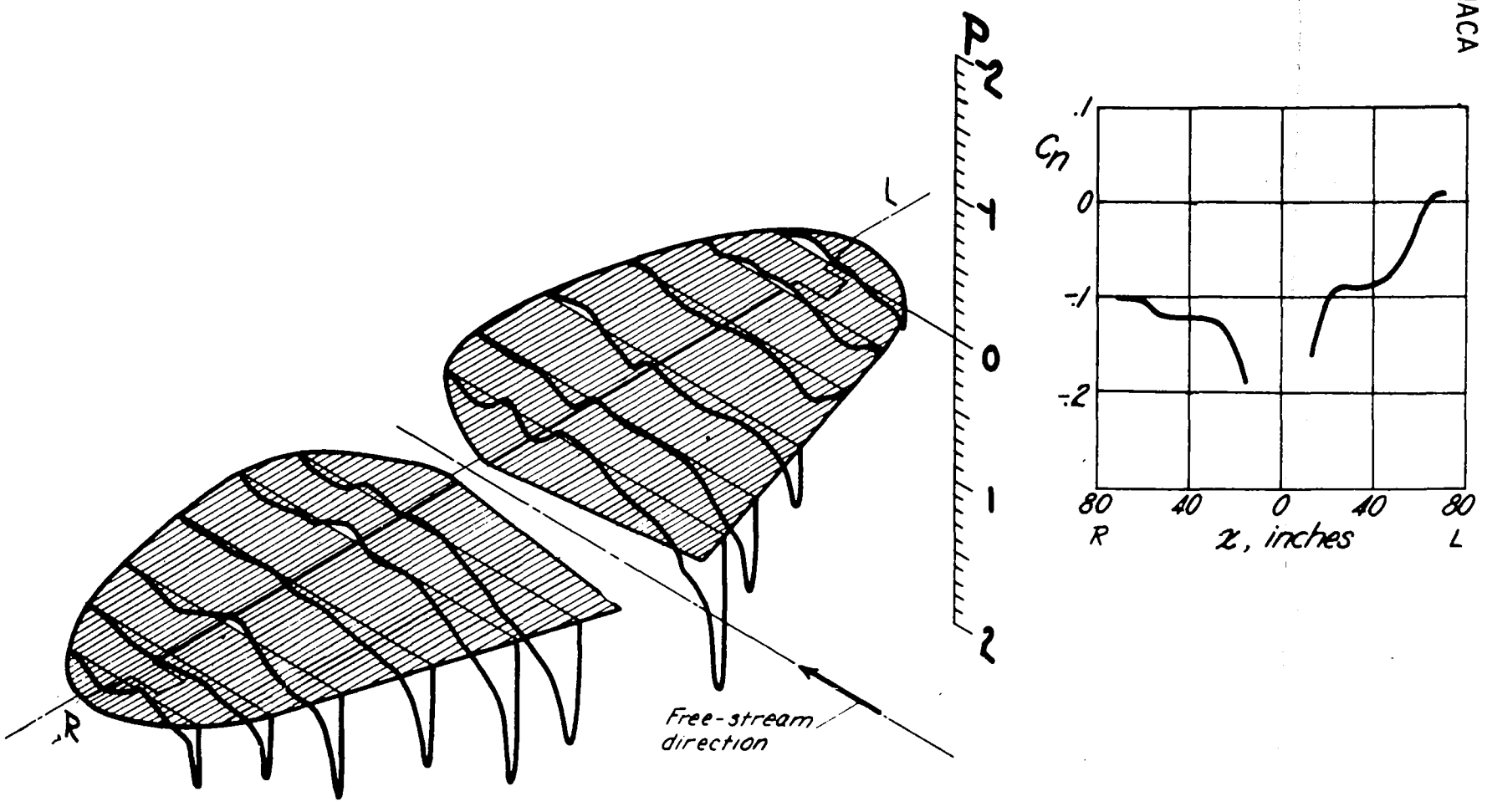

Figure 7.- Pressure distribution over the P-40K horizontal tail, run 1. Propeller removed; C_L, 0.066; ψ, 0°; δ_e, -0.4°.

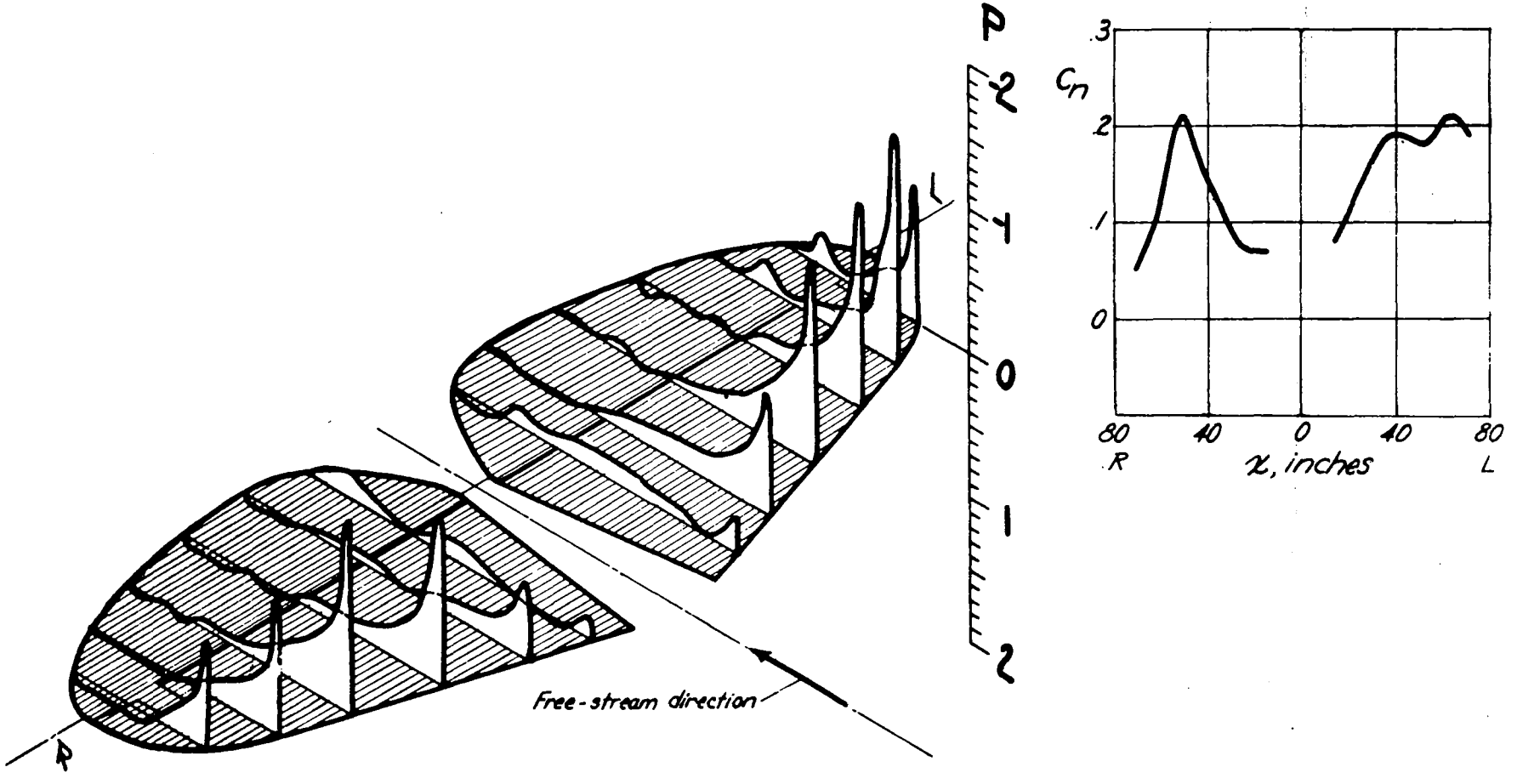

Figure 8.- Pressure distribution over the P-40K horizontal tail, run 3. Propeller removed; C_L, 0.820; ψ, 0°; δ_e, -1.0°.

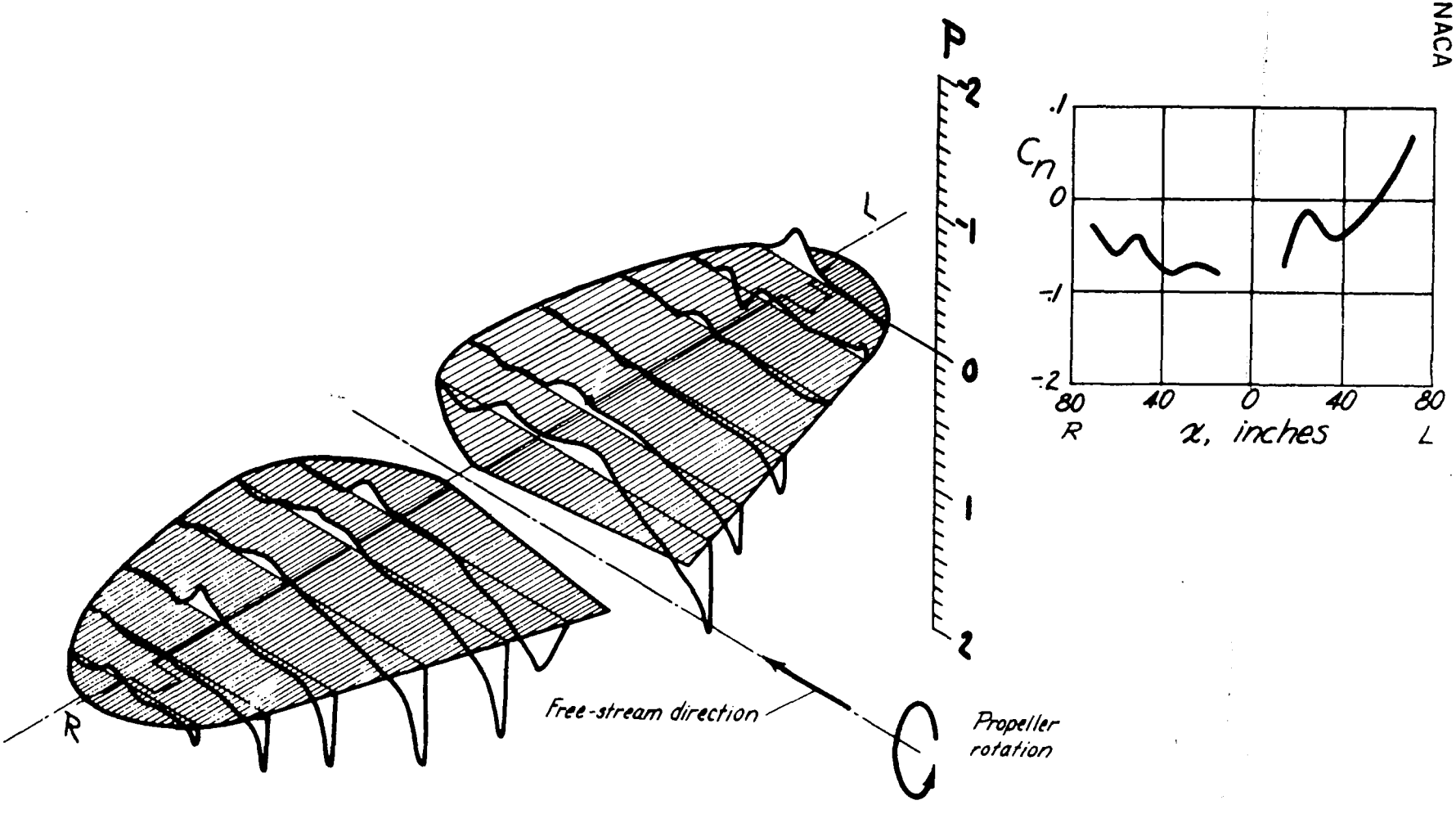

Figure 9.- Pressure distribution over the P-40K horizontal tail, run 10. C_L, 0.066; ψ, 0°; δ_e, -0.4°; β, 35°; V/nD, 1.70.

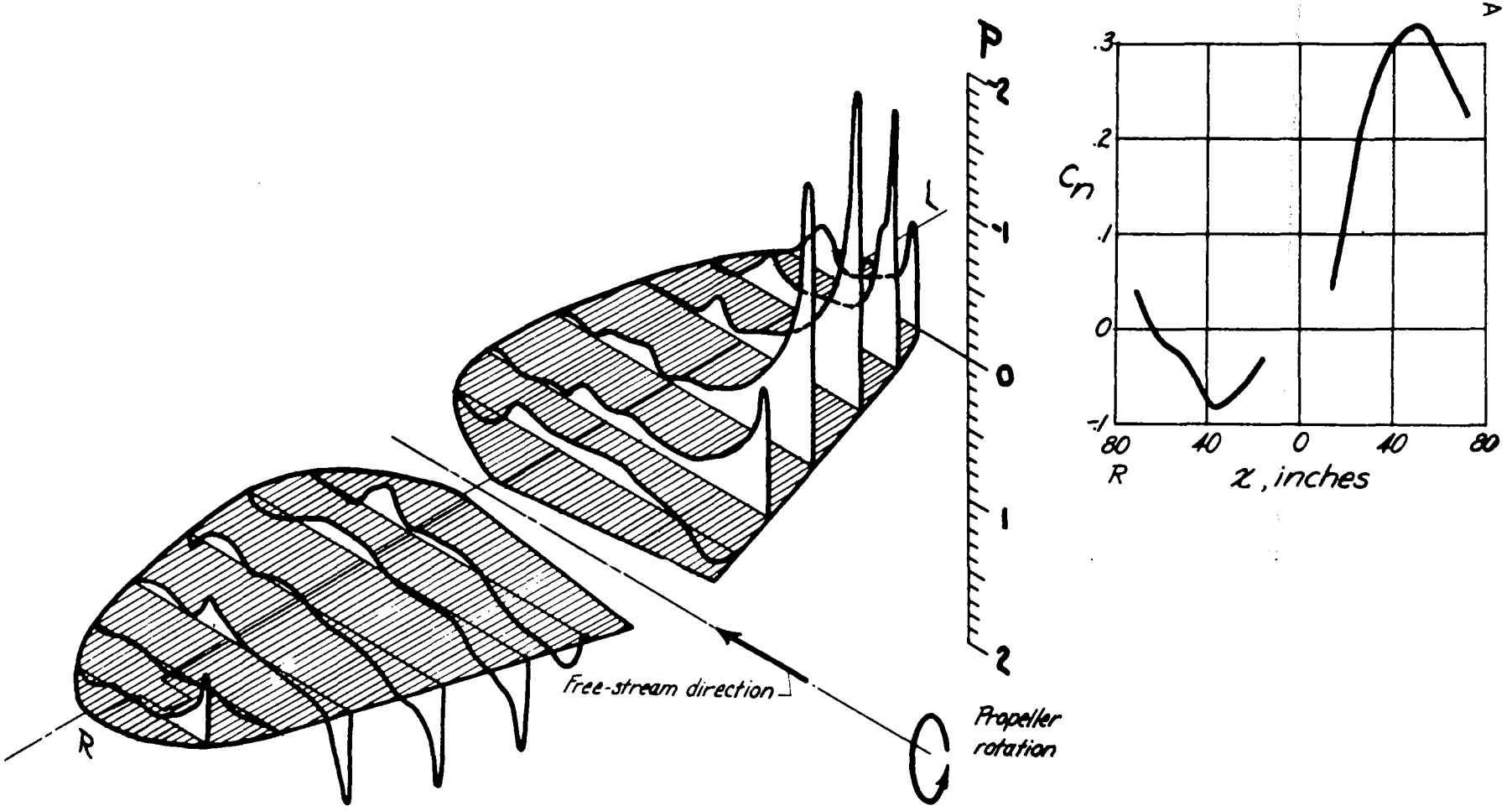

Figure 10.- Pressure distribution over the P-40K horizontal tail, run 17. C_L, 0.820; Ψ, 0°; δ_e, -4.0°; β, 3.5°; V/nD, 0.99.

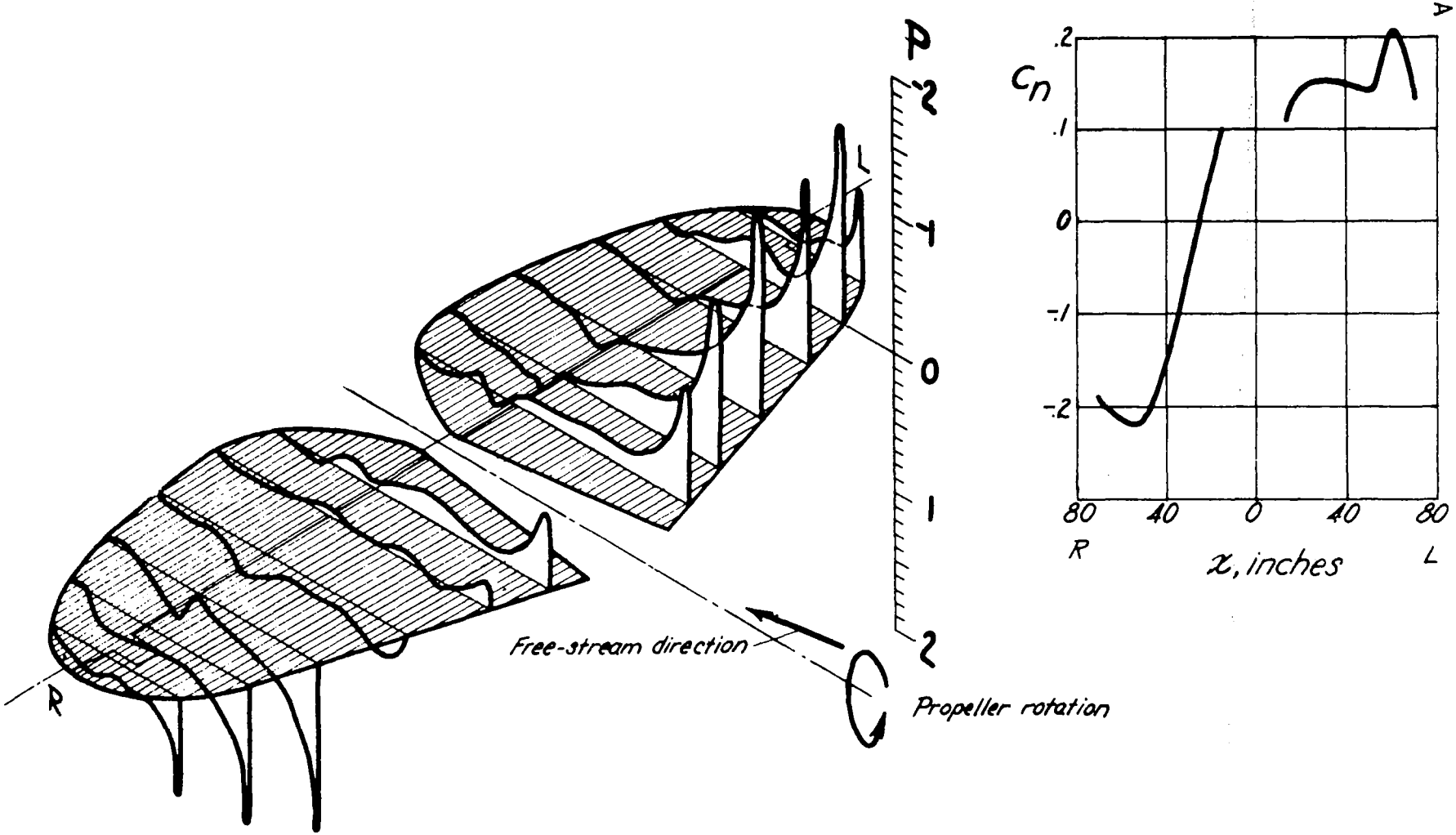

Figure 11.- Pressure distribution over the P-40K horizontal tail, run 30.
C_t, 0.820; ψ, 5°; δ_e, -1.0°; β, 35°; V/nD, 0.99.

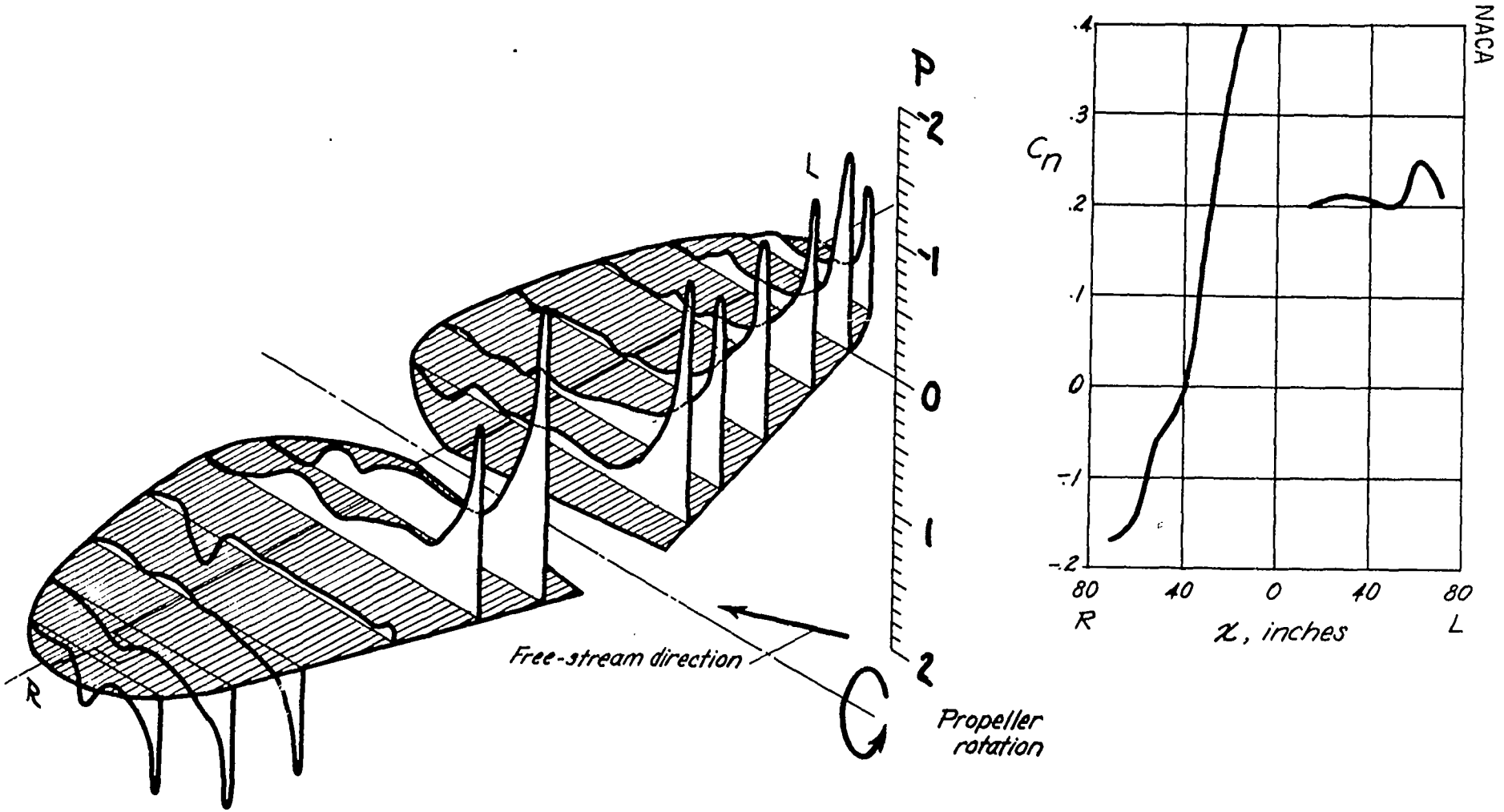

Figure 12.– Pressure distribution over the P-40K horizontal tail, run 42. C_L, 0.820; ψ, 10°; δ_e, -1.0°; β, 35°; V/nD, 0.99.

Fig. 12

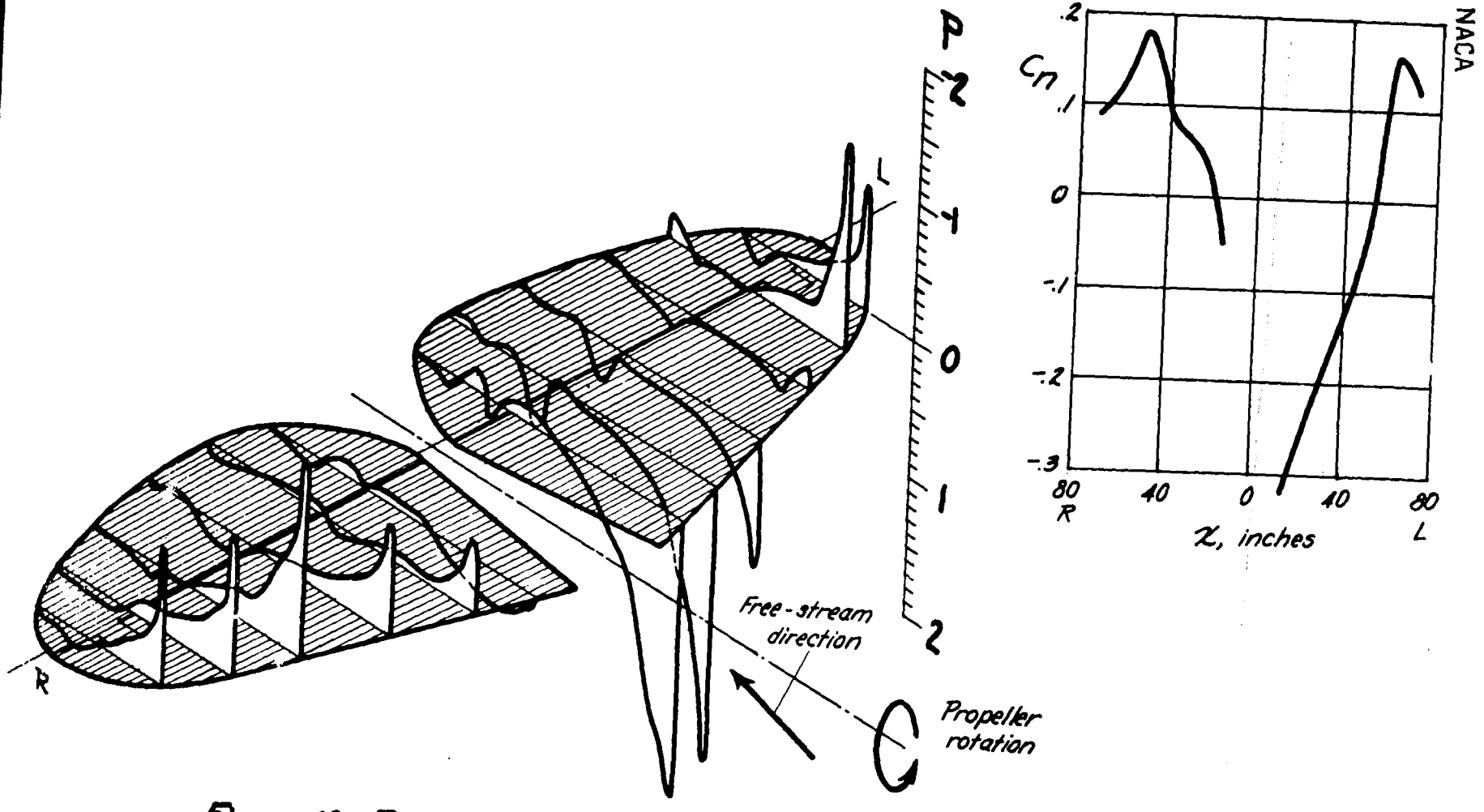

Figure 13.- Pressure distribution over the P-40K horizontal tail, run 52. C_L, 0.820; ψ, -10°; δ_e, -1.0°; β, 35°; V/nD, 0.99.

Fig. 13

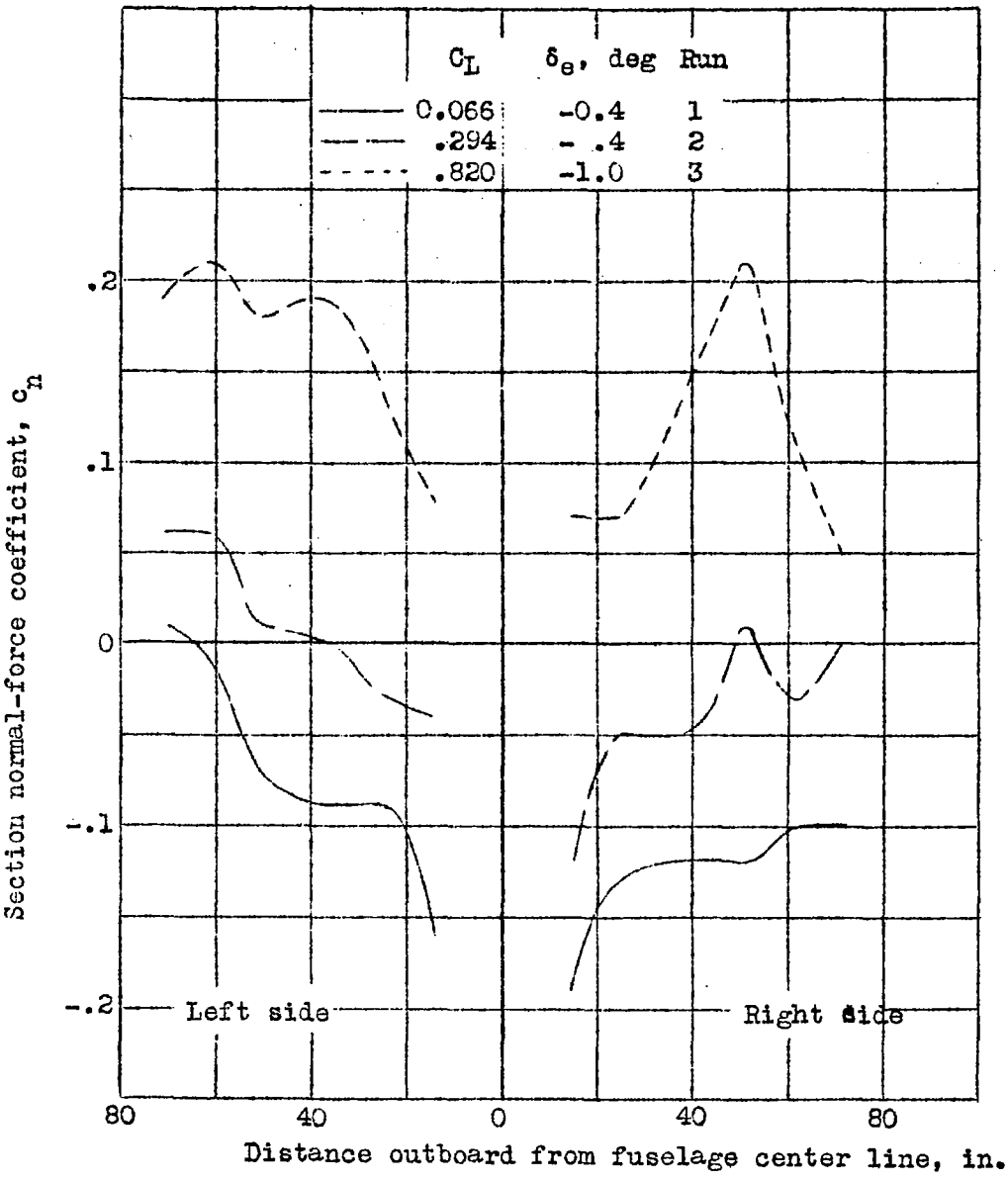

Figure 14.- Spanwise variation of tail normal-force coefficient. Propeller removed; ψ, 0°.

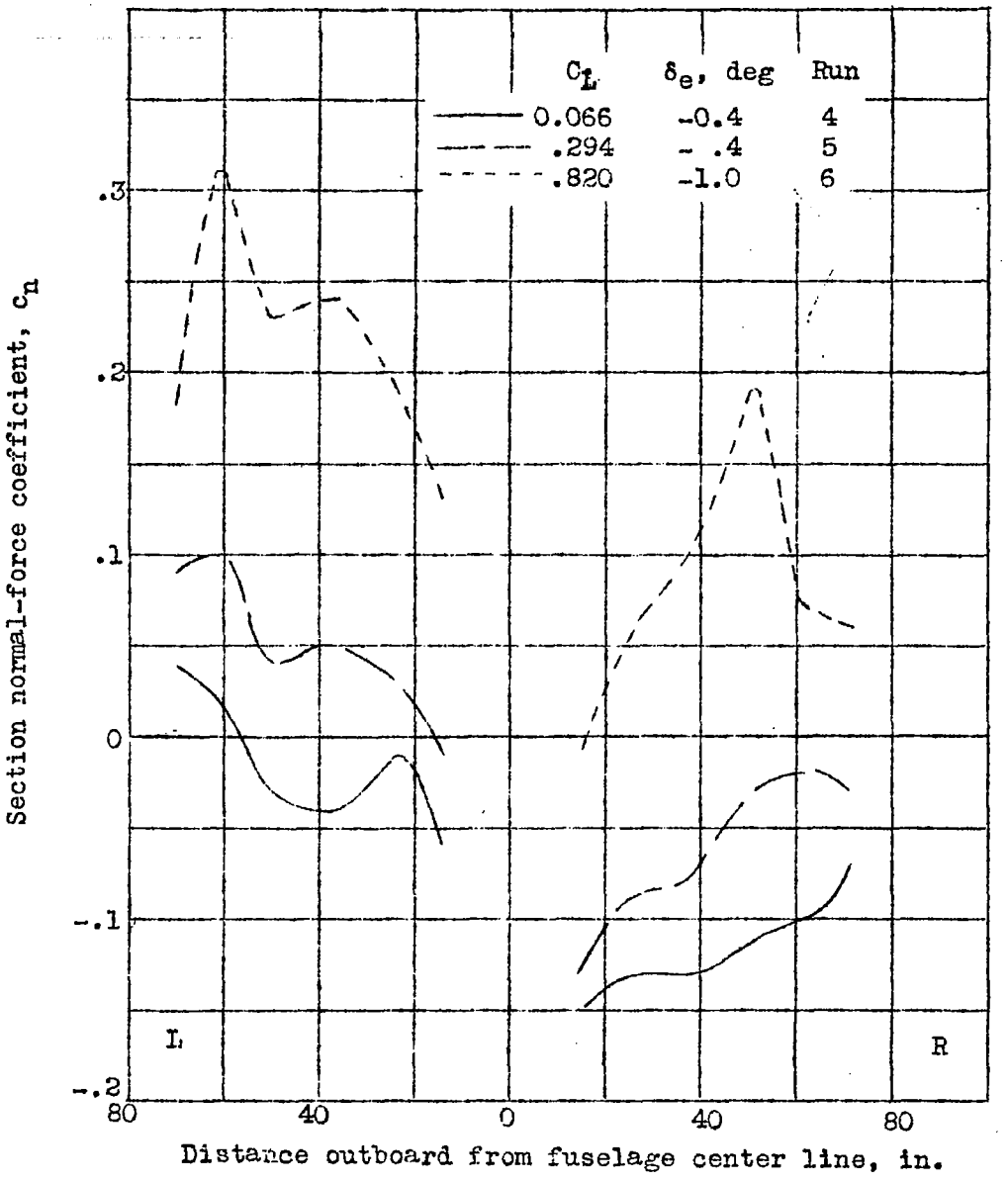

Figure 15.- Spanwise variation of tail normal-force coefficient. Propeller removed; ψ, 5°.

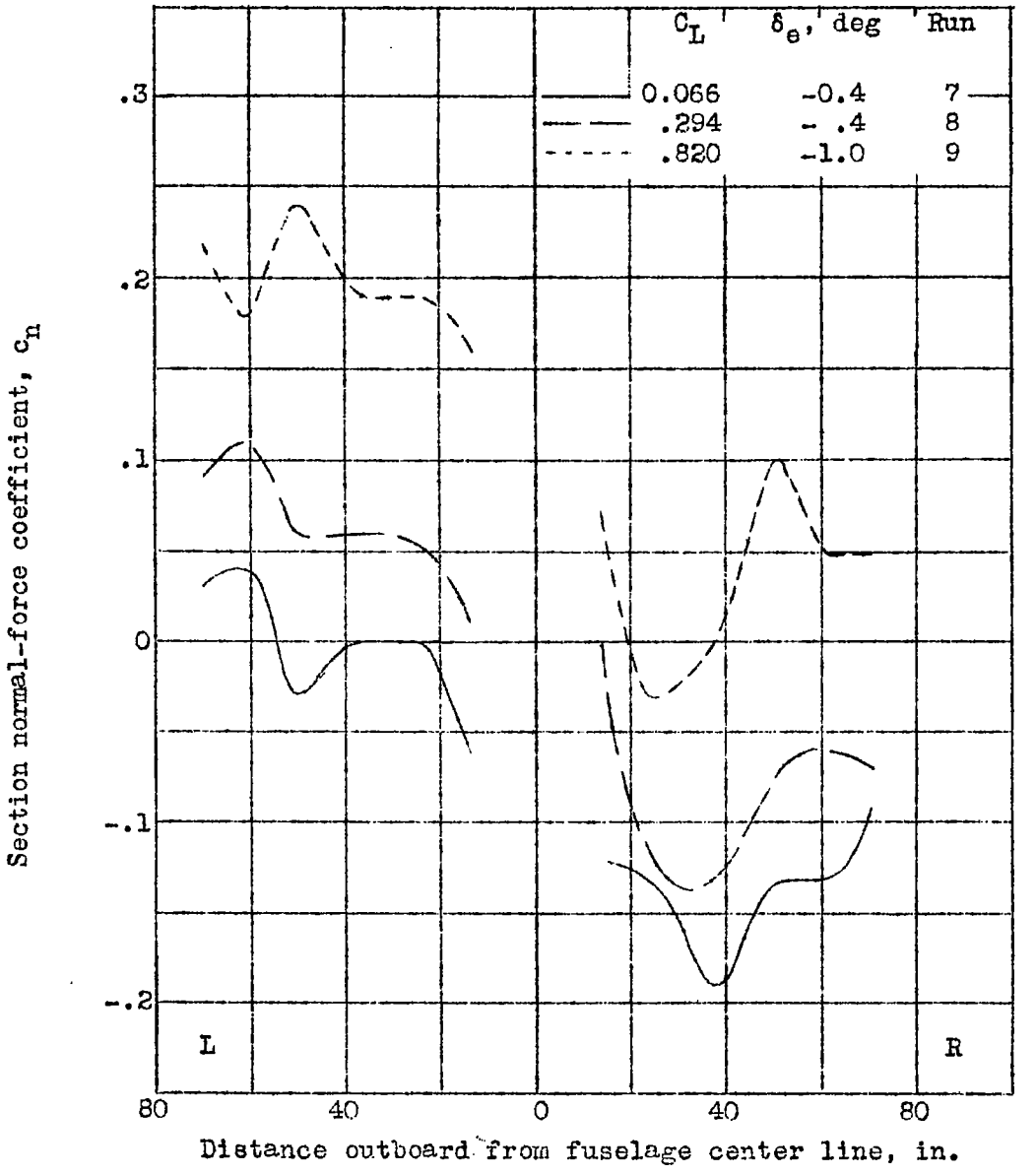

Figure 16.- Spanwise variation of tail normal-force coefficient. Propeller removed; ψ, 10°.

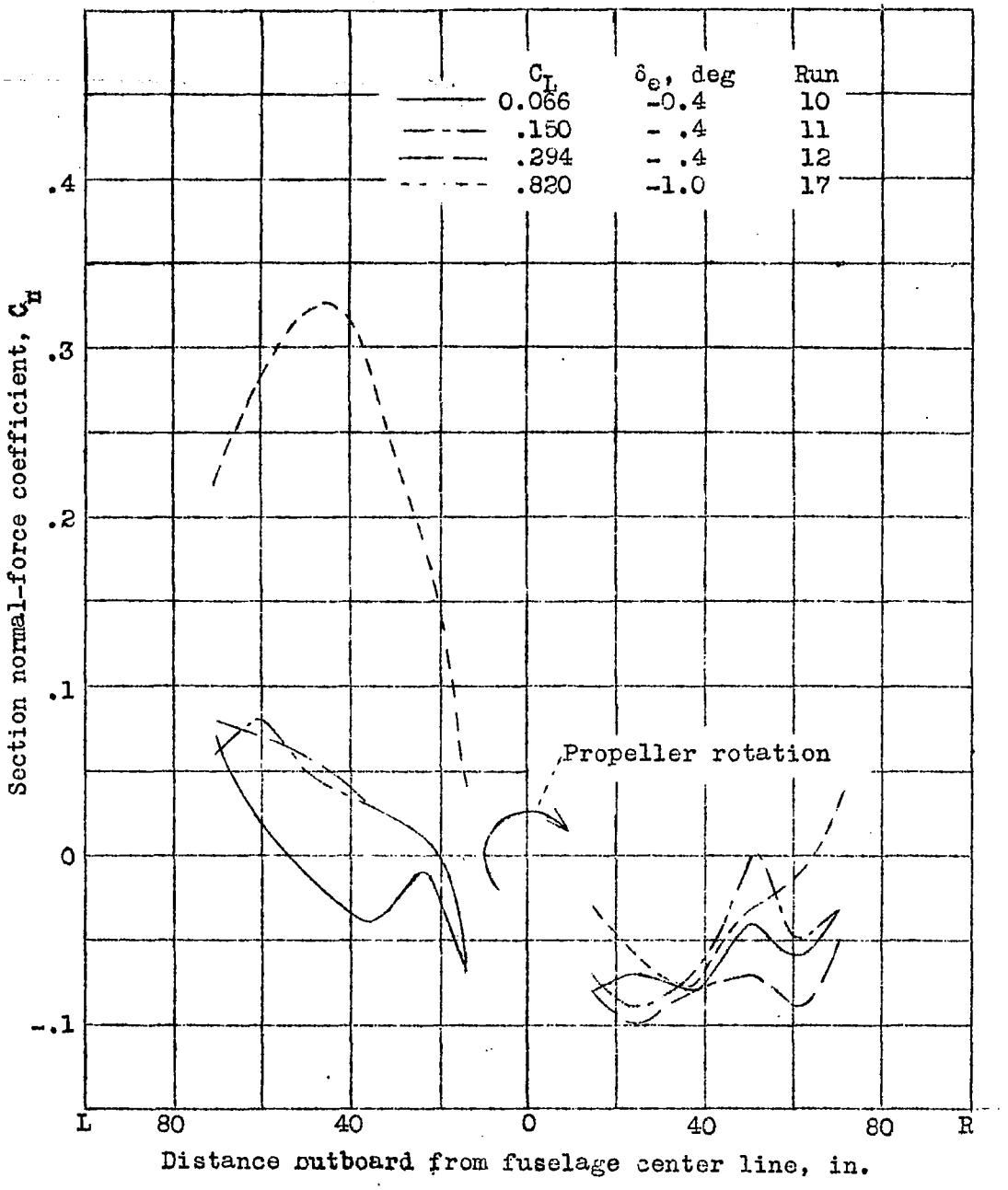

Figure 17.- Spanwise variation of tail normal-force coefficient. Rated power; ψ, 0°.

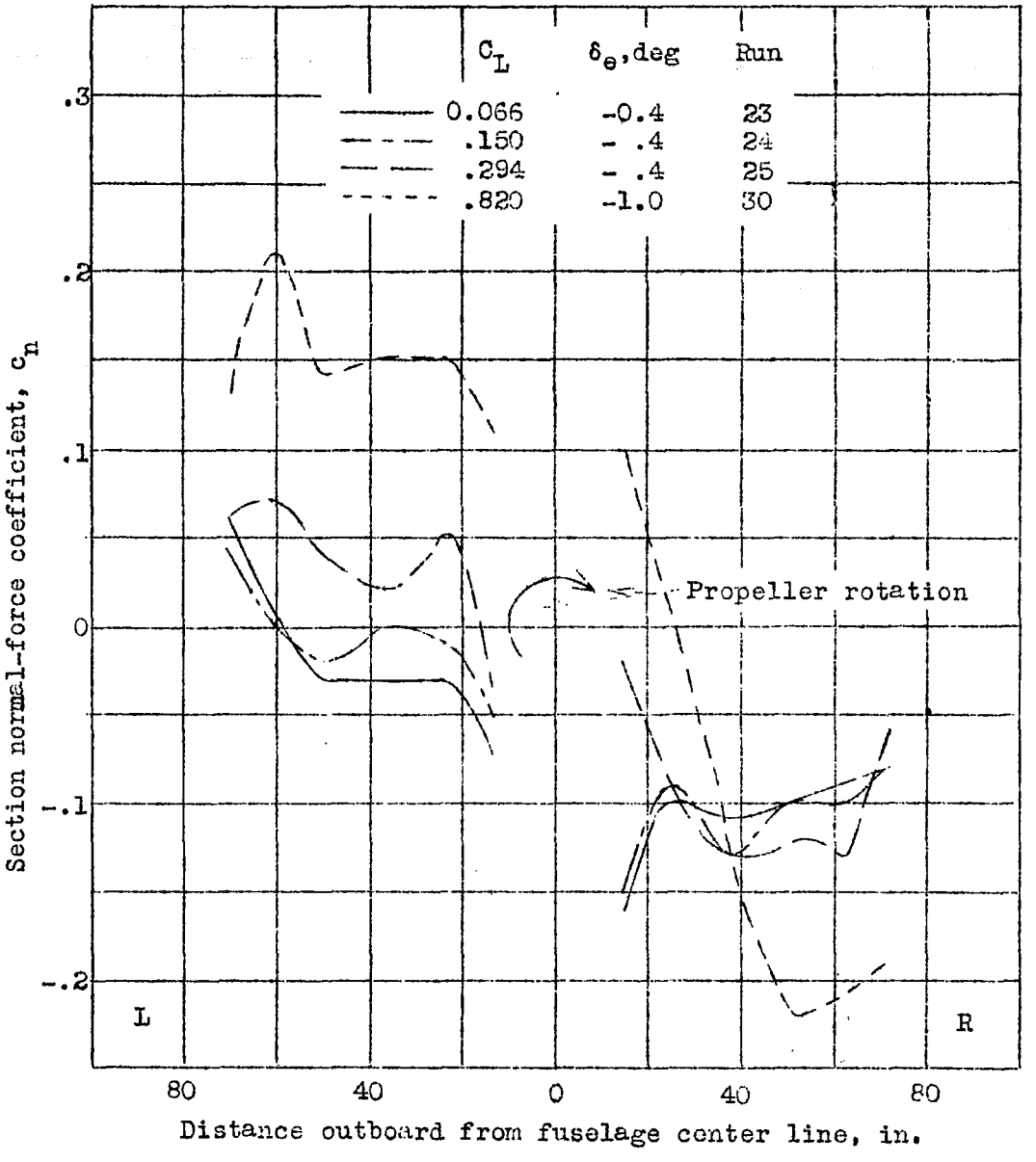

Figure 18.- Spanwise variation of tail normal-force coefficient. Rated power; ψ, 5°.

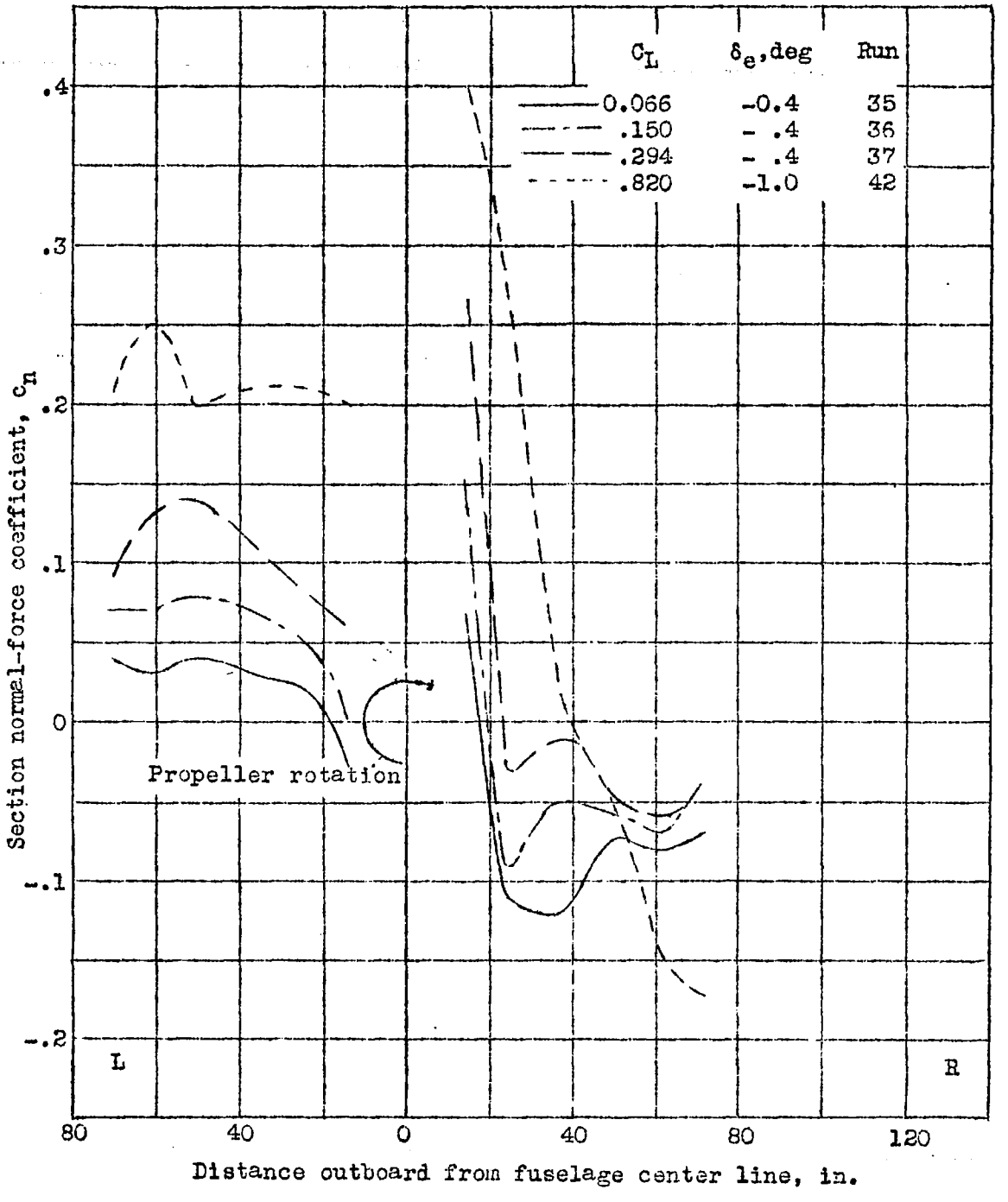

Figure 19.- Spanwise variation of tail normal-force coefficient. Rated power; ψ, 10°.

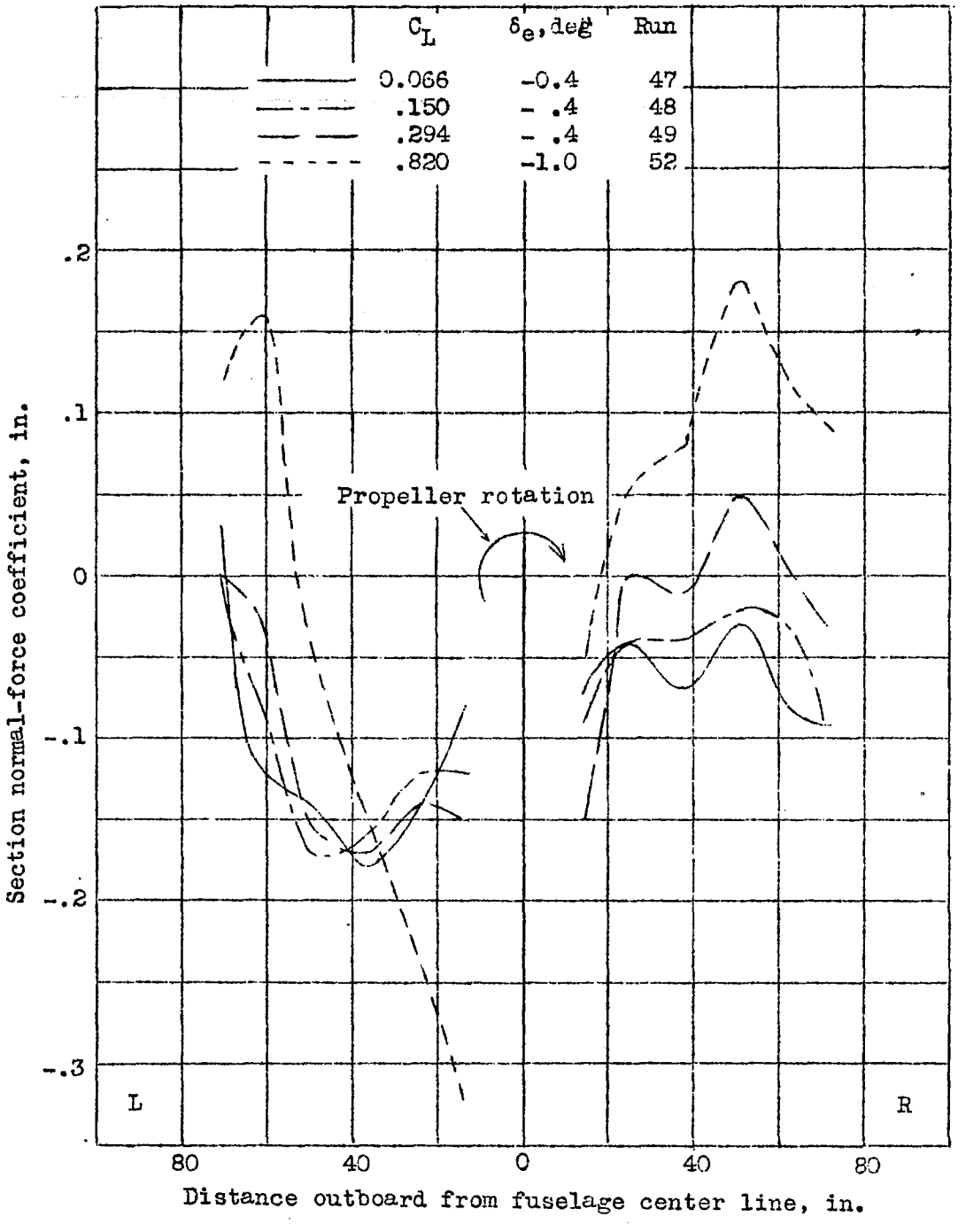

Figure 20.- Spanwise variation of tail normal-force coefficient. Rated power; ψ, -10°.

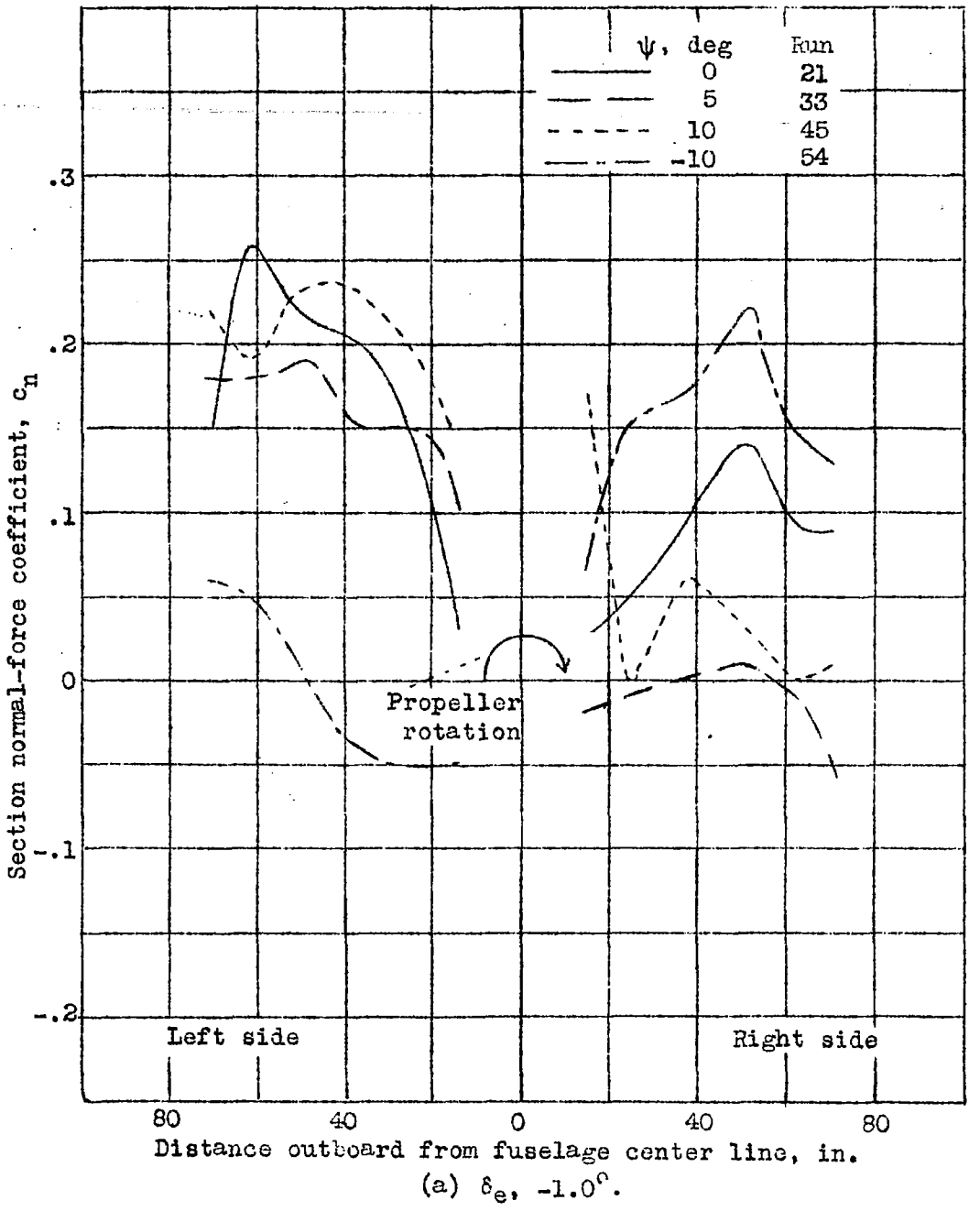

(a) δ_e, -1.0°.

Figure 21.- Spanwise variation of tail normal-force coefficient. Rated power; n, 9.02; C_L, 0.820.

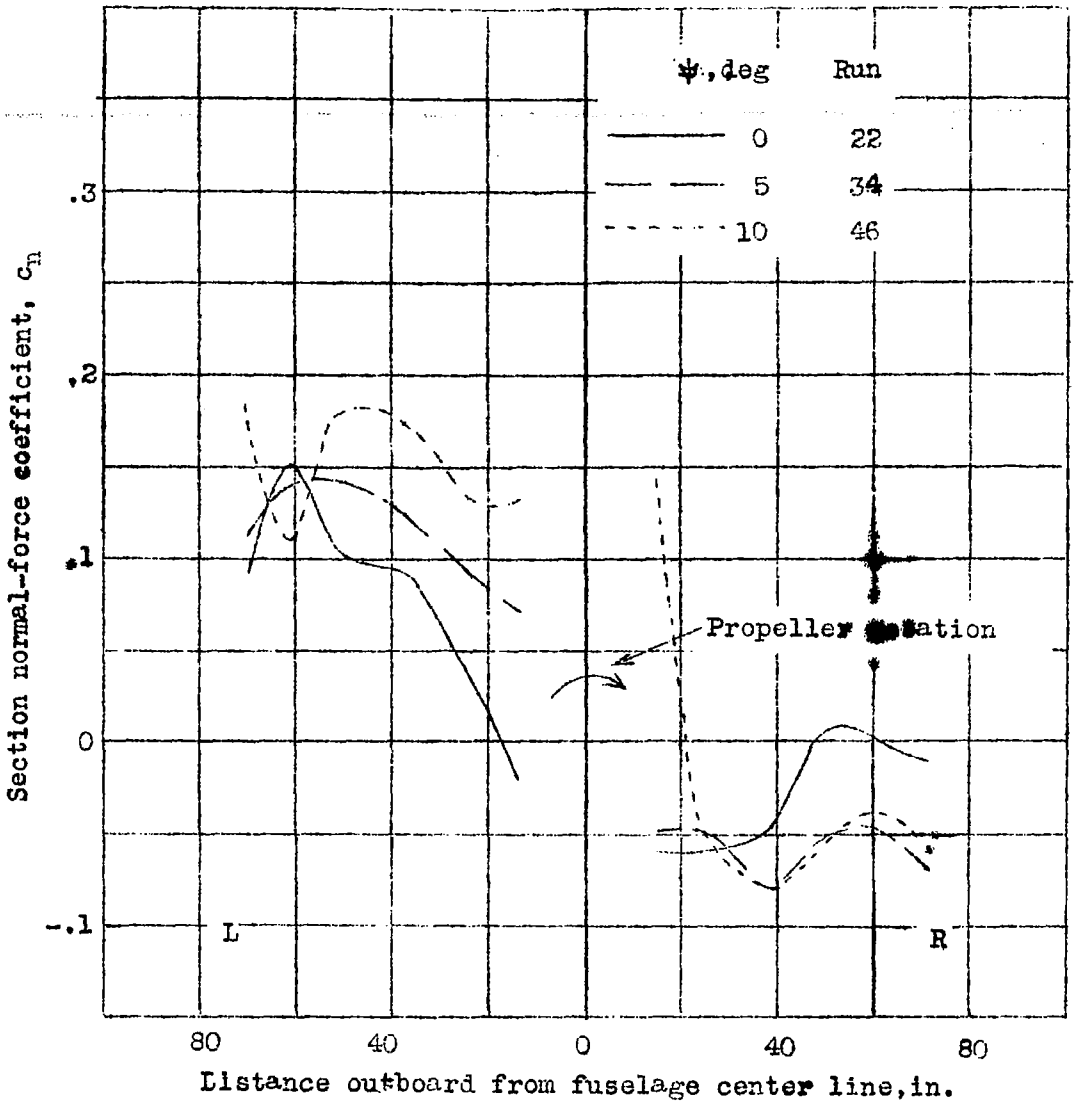

(b) δ_e, -5.0°

Figure 21.- Concluded.

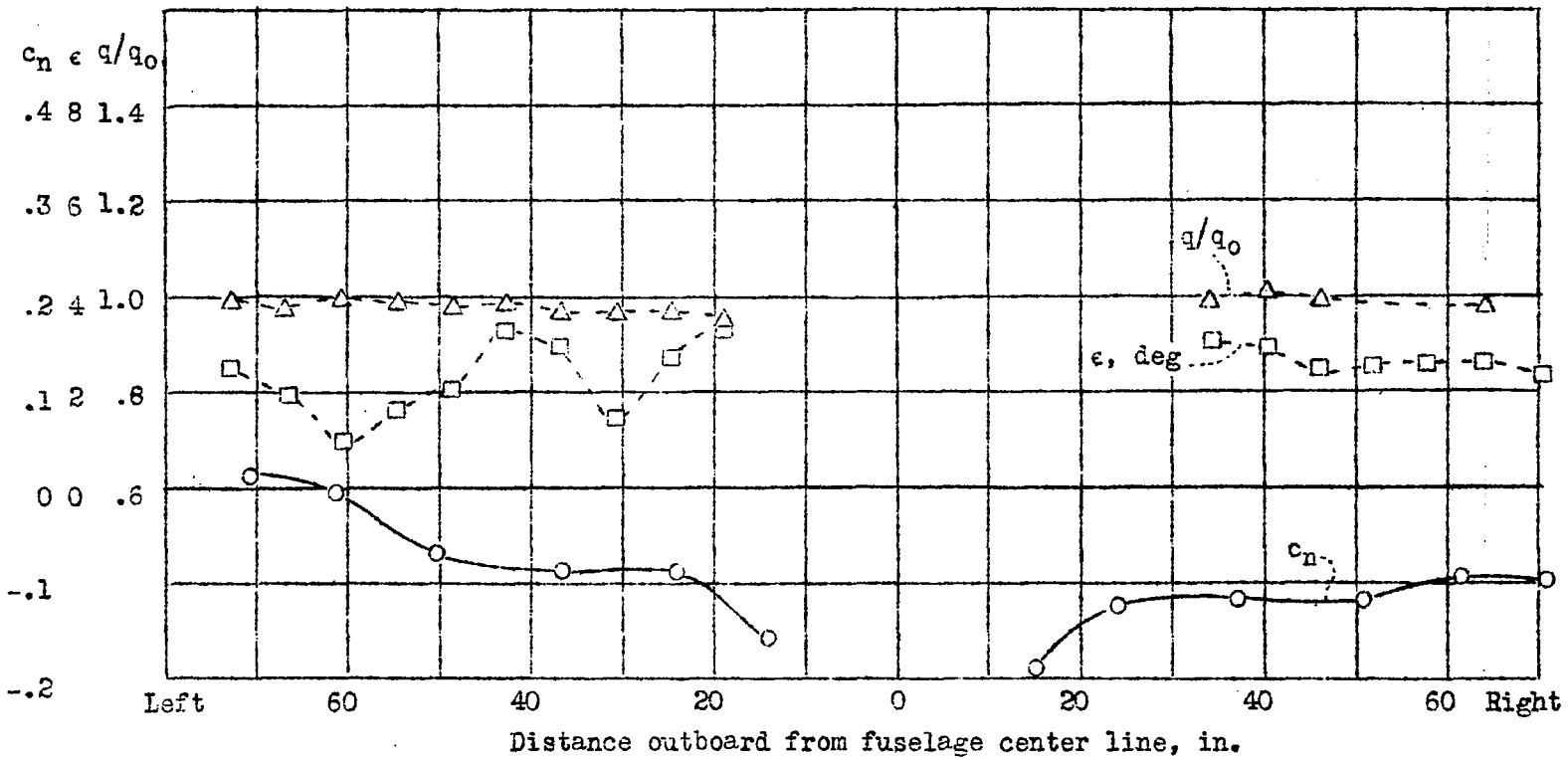

Figure 22.- Variation of c_n, ε, and q/q_o across the horizontal tail span. ψ, 0°; C_L, 0.066; δ_e, -0.4°; propeller removed; run 1.

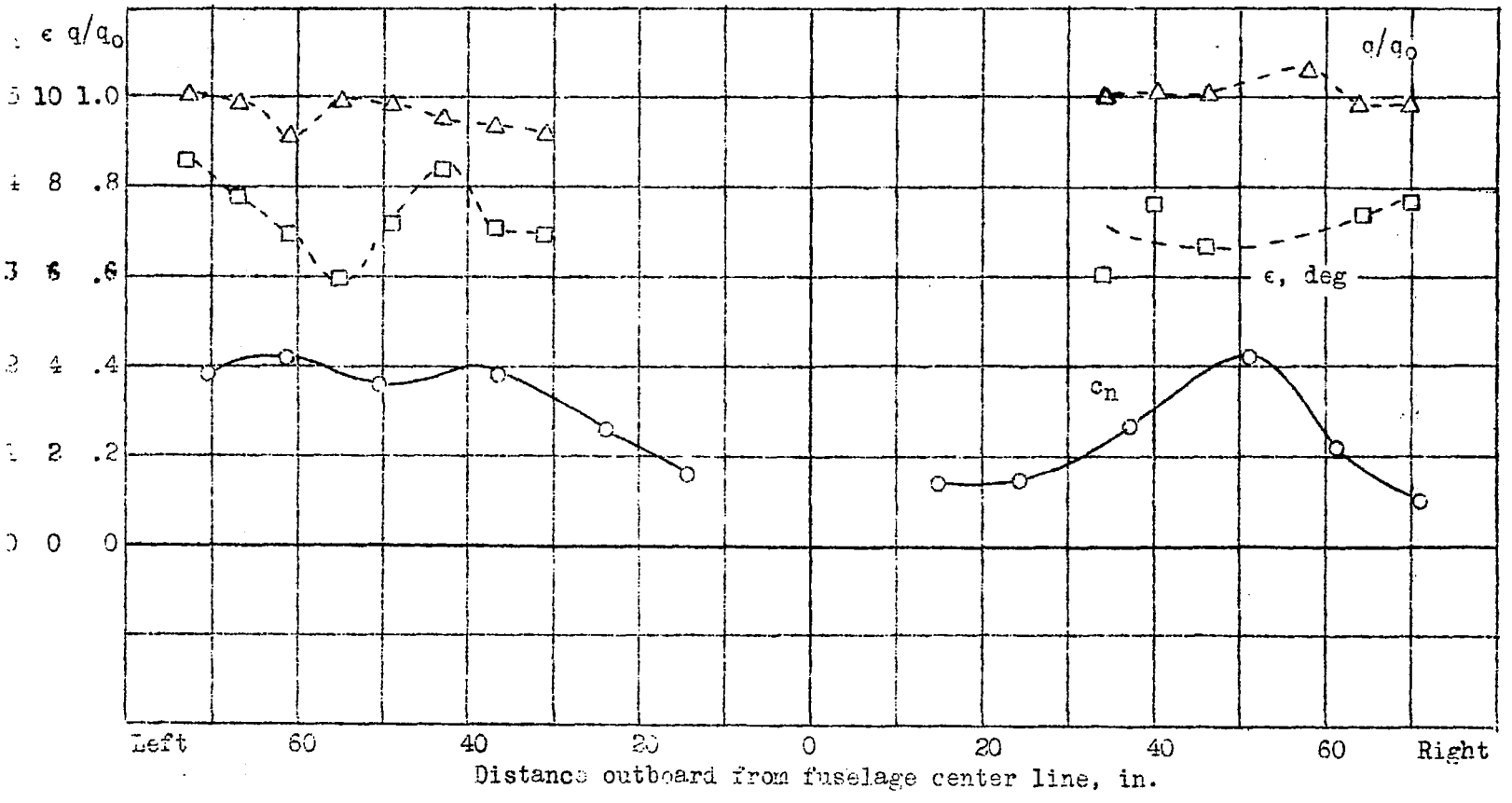

Figure 23.- Variation of c_n, ϵ, and q/q_o across the horizontal tail span. ψ, 0°; C_L, 0.820; δ_e, -1.0°; propeller removed; run 3.

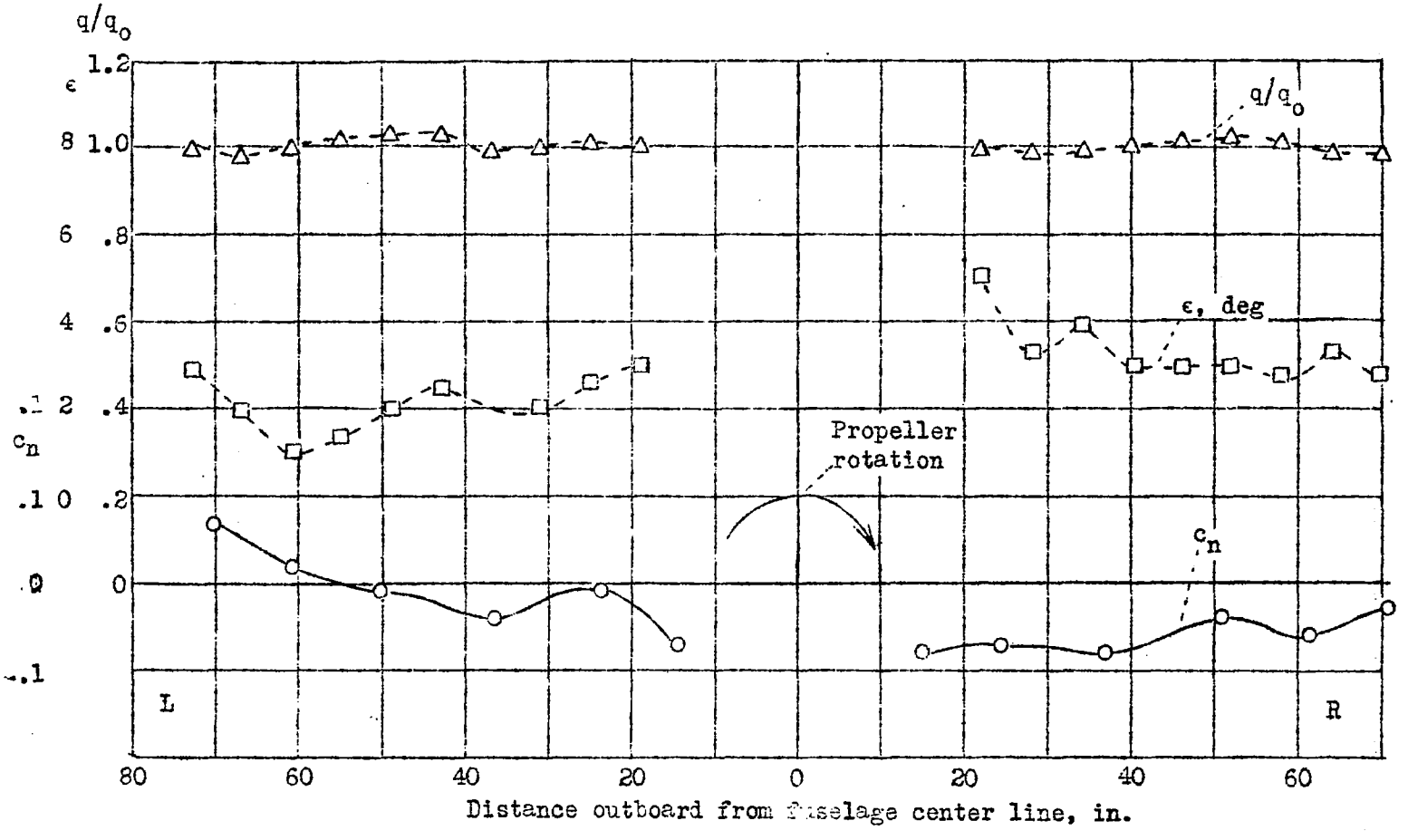

Figure 24.- Variation of c_n, ϵ, and q/q_o across the horizontal tail span. ψ, 0°; C_L, 0.066; δ_e, -0.4°; V/nD, 1.70; β,35°; run 10.

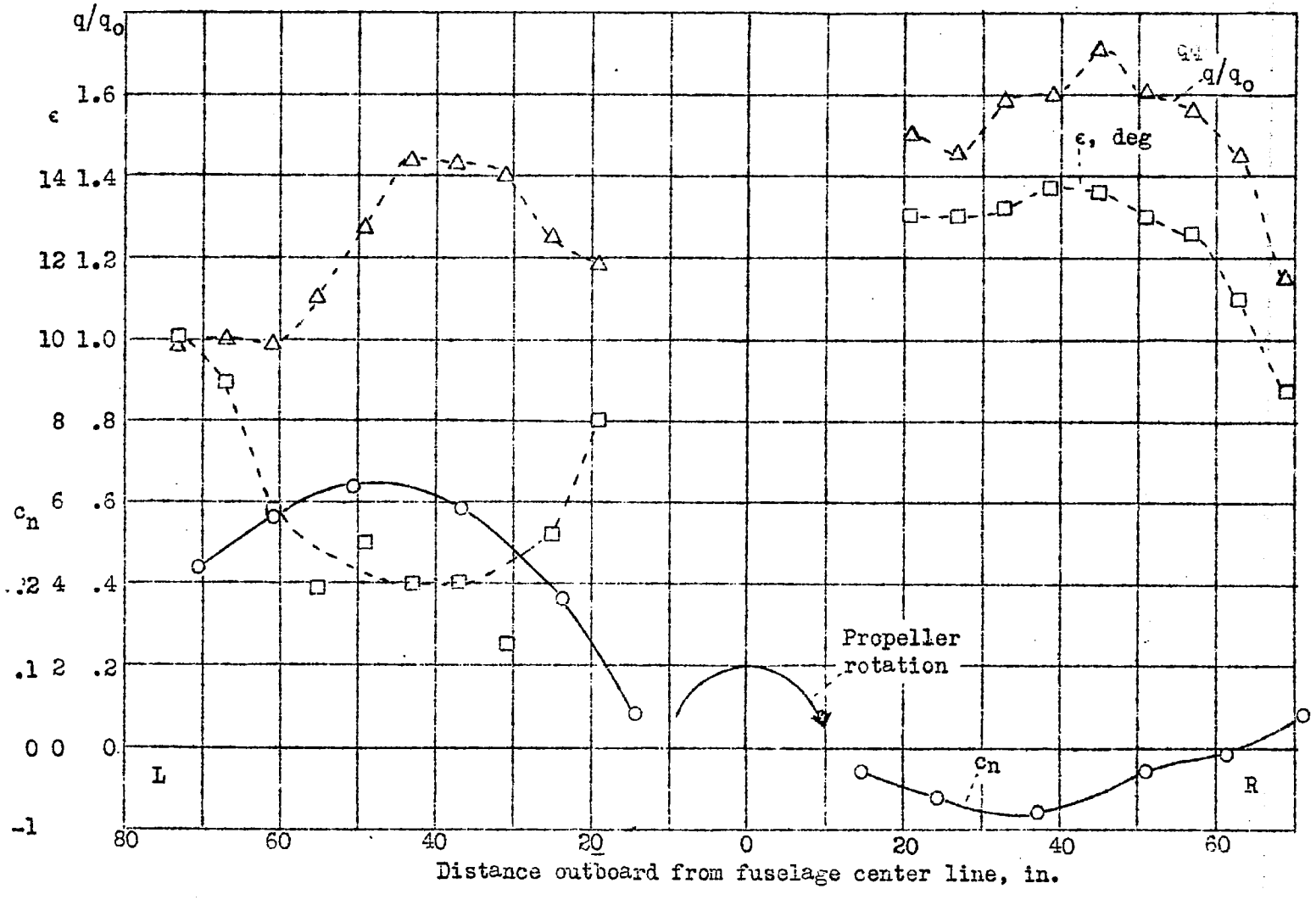

Figure 25.- Variation of c_n, ϵ, and q/q_o across the horizontal tail span. ψ, 0°; C_L, 0.820; δ_e, -1.0°; V/nD, 0.99; β,35°; run 17.

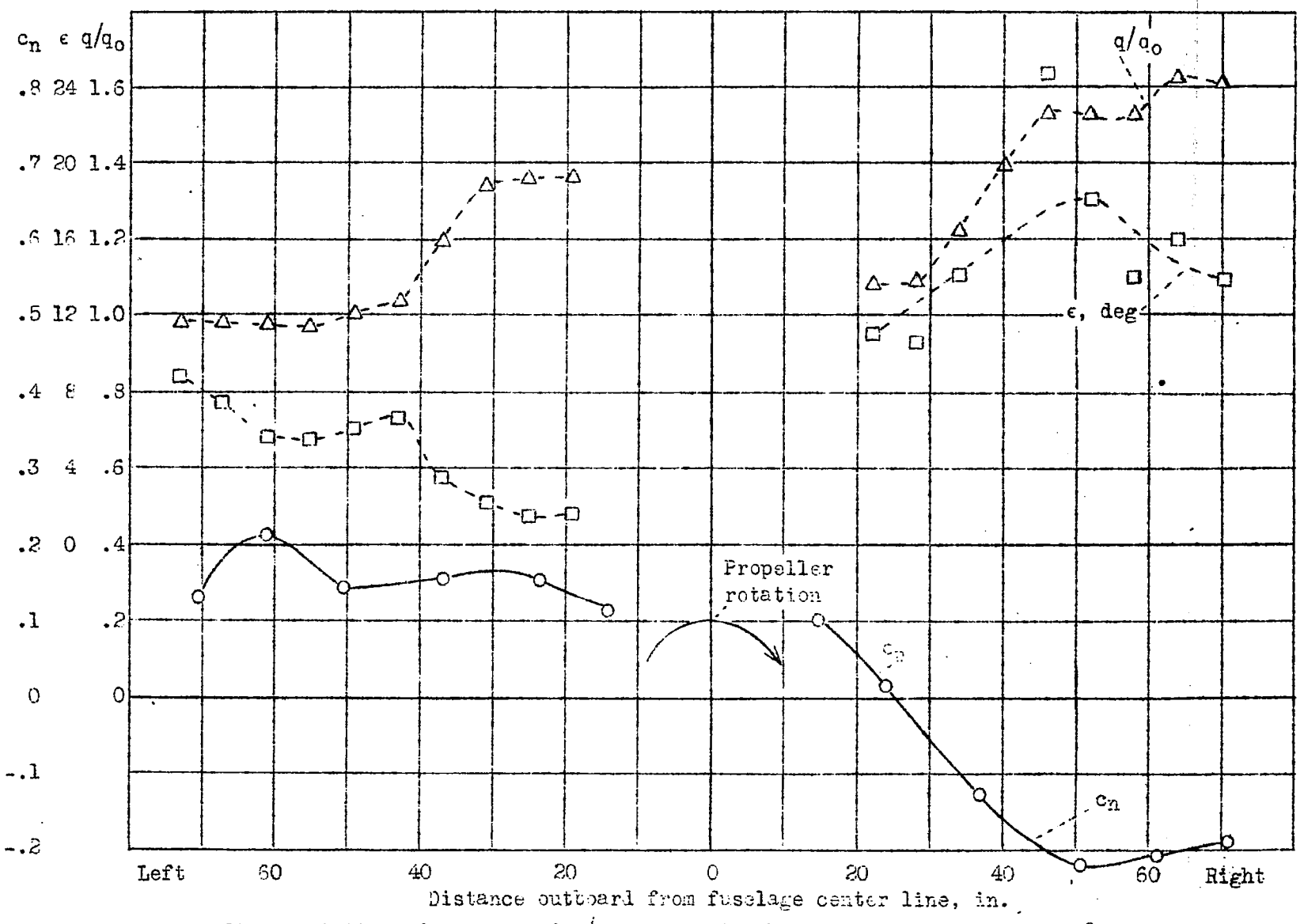

Figure 26.- Variation of c_n, ε, and q/q_o across the horizontal tail span. ψ, 5°; C_L, 0.820; δ_e, -1.0°; V/nD, 0.99; β, 35°; run 30.

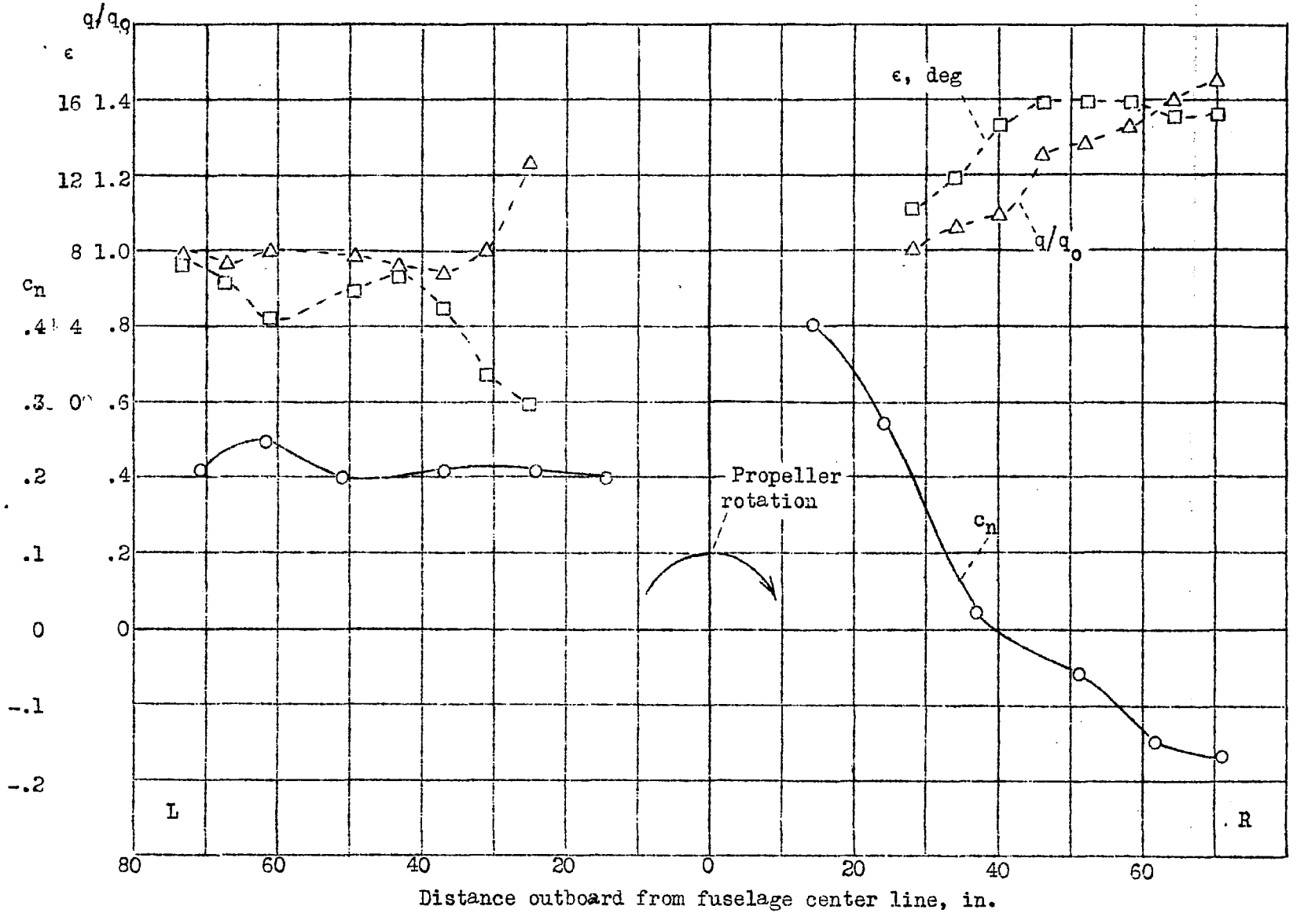

Figure 27.- Variation of c_n, ϵ, and q/q_o across the horizontal tail span. ψ,10°; C_L,0.820; δ_e, -1.0°; V/nD, 0.99; β, 35°; run 42.

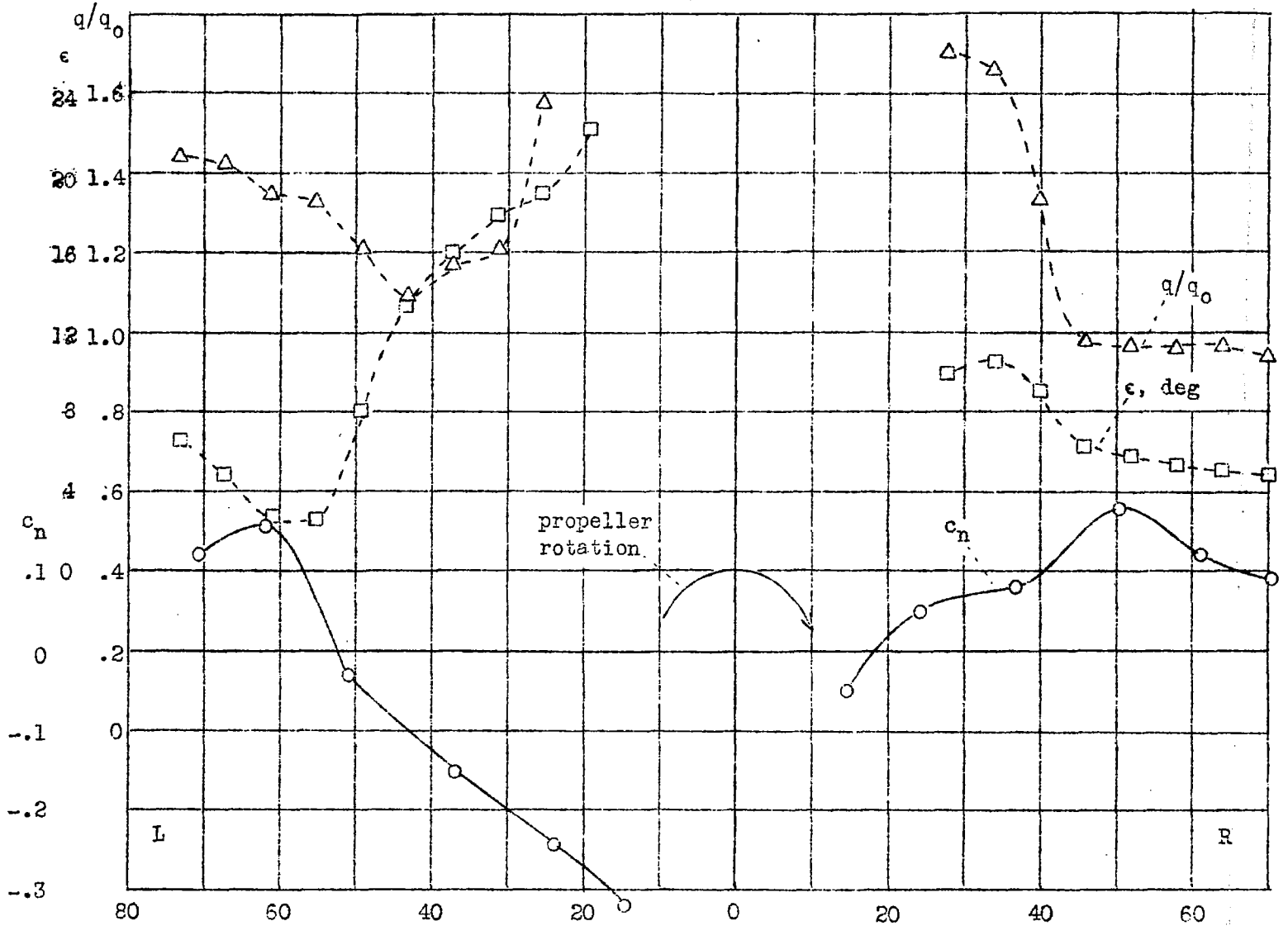

Figure 28.- Variation of c_n, ϵ, and q/q_o across the horizontal tail span. ψ, -10°; C_L, 0.820; δ_e, -1.0°; V/nD, 0.99; β, 35°; run 52.

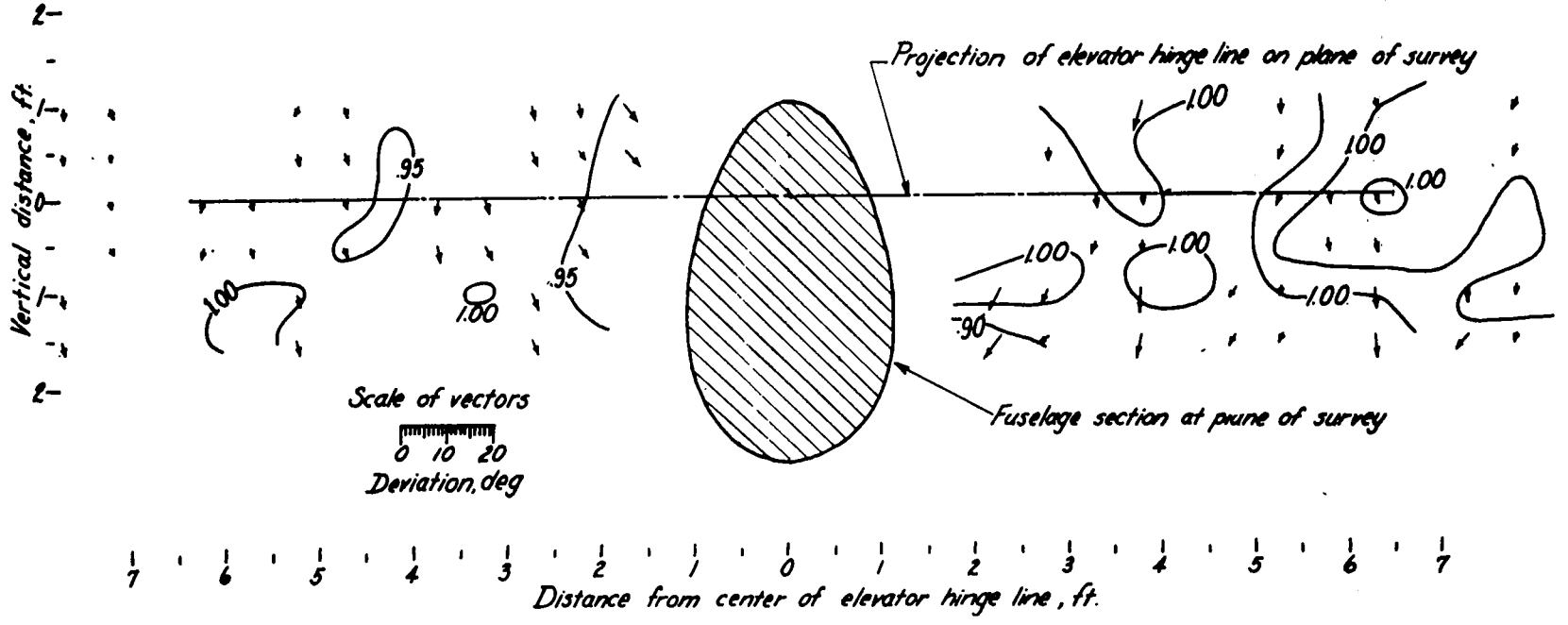

Figure 29. — Dynamic-pressure (q/q_0) contours and inclination of the air stream in a vertical plane 7.25 feet forward of the elevator hinge line, measured along thrust axis. Vectors show angular deviation of air flow from the free-stream direction. View looking forward. Propeller removed. Run 1; C_L, 0.066; Ψ, 0°.

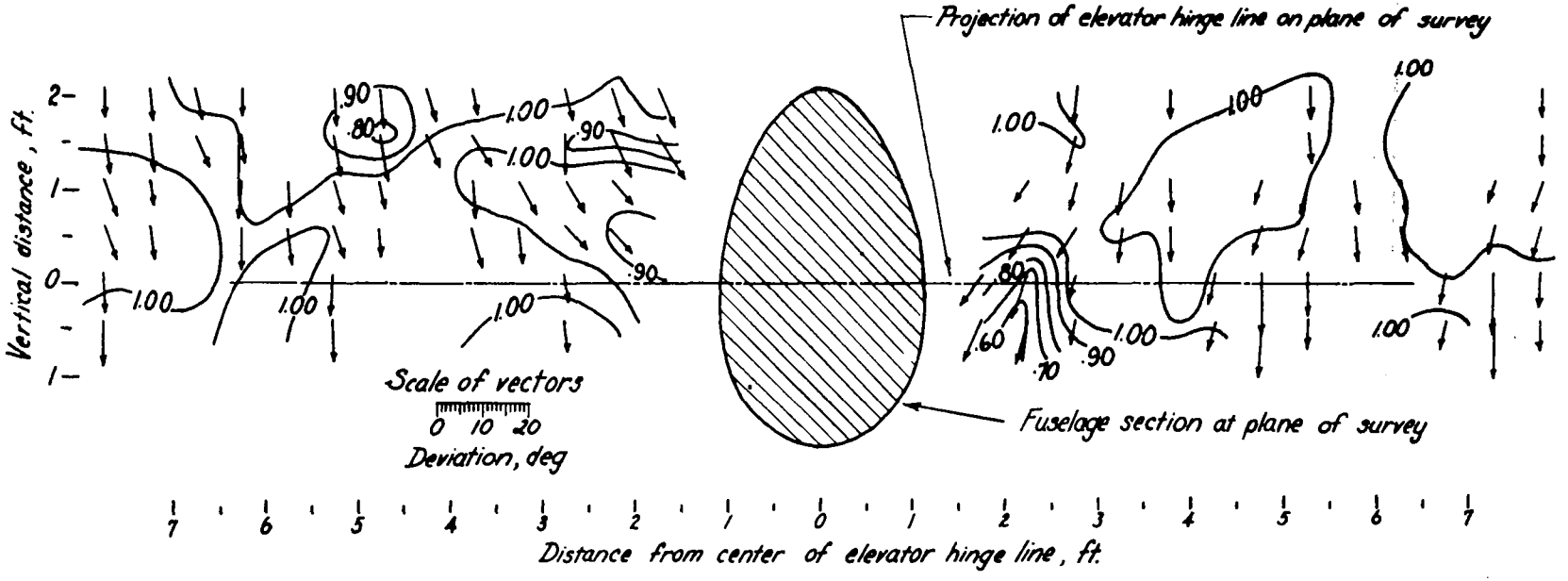

Figure 30.— Dynamic-pressure(q/q_0) contours and inclination of the air stream in a vertical plane 7.25 feet forward of the elevator hinge line, measured along thrust axis. Vectors show angular deviation of air flow from the free-stream direction. View looking forward. Propeller removed. Run 3; C_L, 0.820; ψ, 0°.

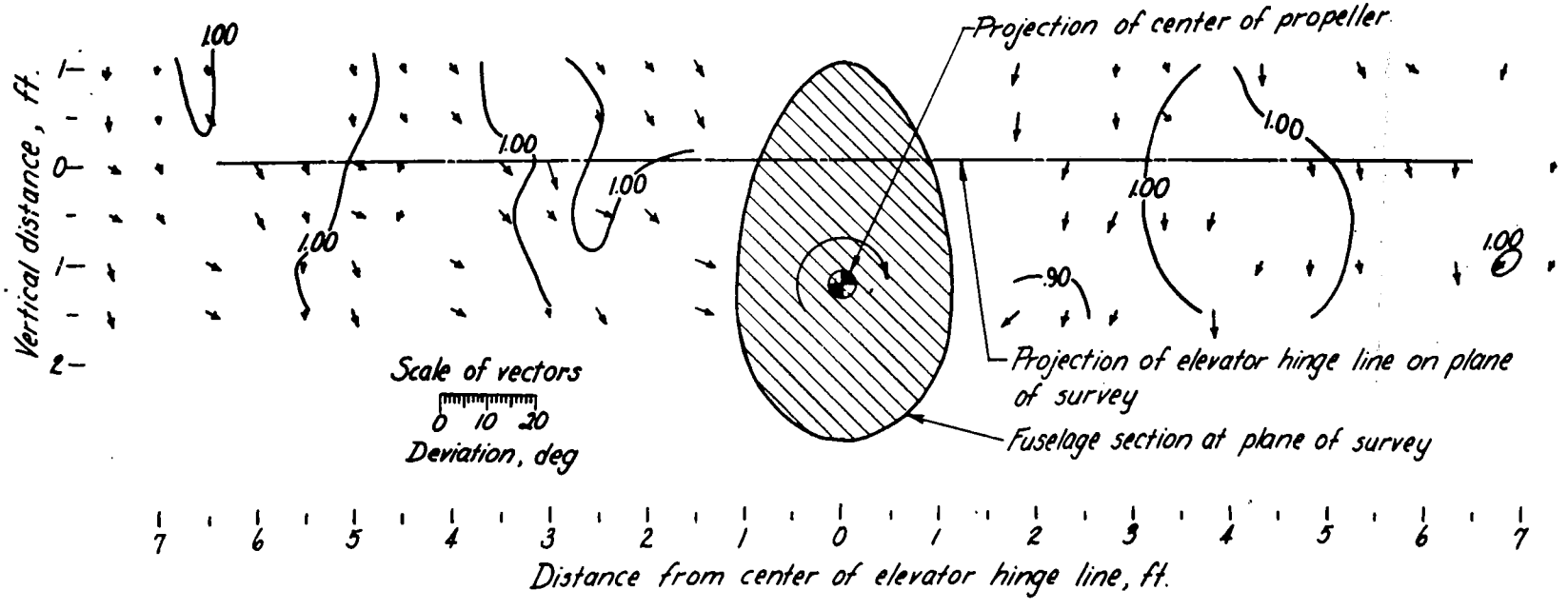

Figure 31.—Dynamic-pressure (q/q_0) contours and inclination of the air stream in a vertical plane 7.25 feet forward of the elevator hinge line, measured along thrust axis. Vectors show angular deviation of air flow from free-stream direction. View looking forward. Propeller operating. Run 10; C_L, 0.066; ψ, 0°; V/nD, 1.70.

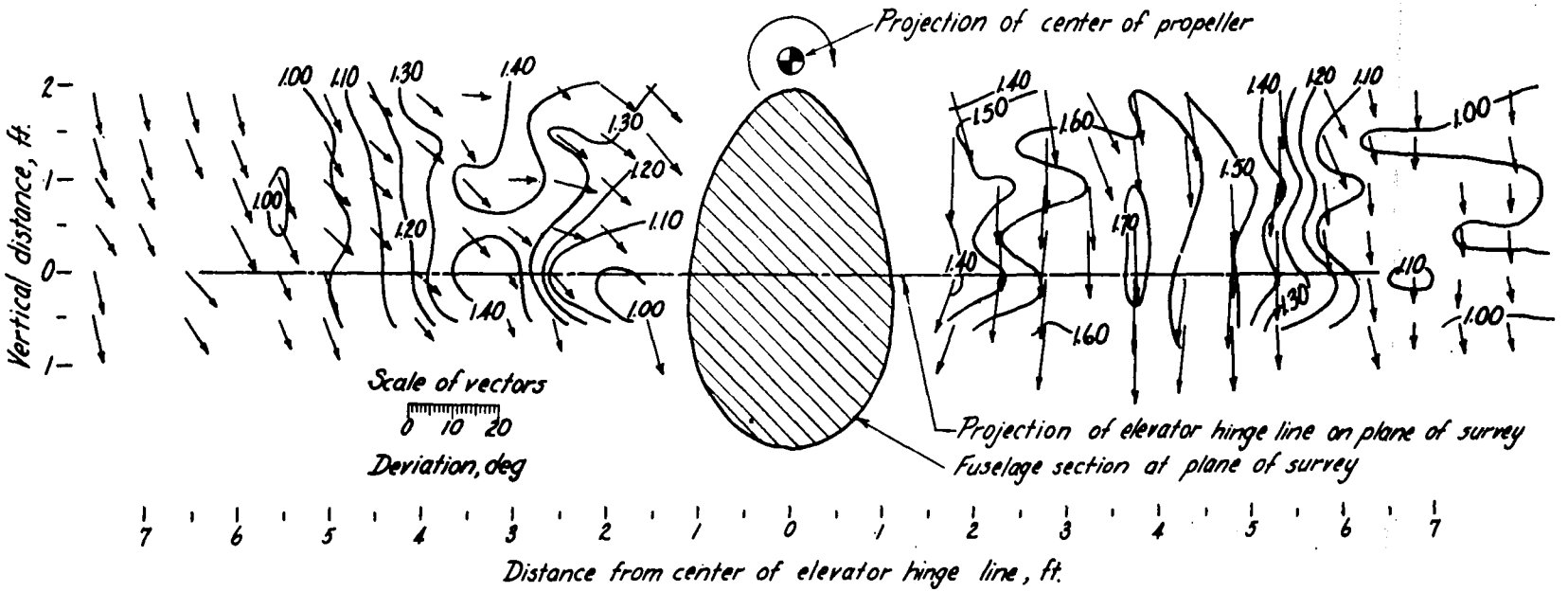

Figure 32.-Dynamic-pressure (q/q_0) contours and inclination of the air stream in a vertical plane 7.25 feet forward of the elevator hinge line, measured along thrust axis. Vectors show angular deviation of air flow from free-stream direction. View looking forward. Propeller operating. Run 17; C_L, 0.820; Φ, 0°; V/nD, 0.99.

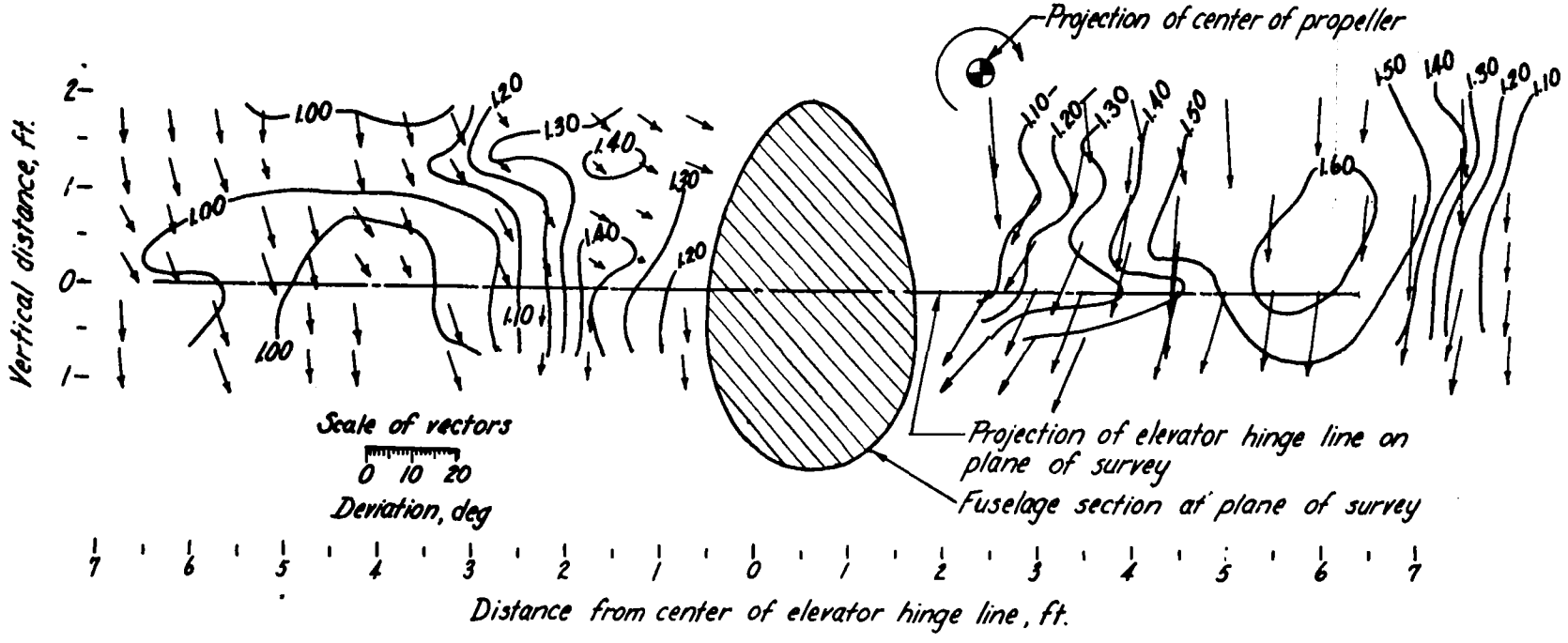

Figure 33.-Dynamic-pressure (q/q_0) contours and inclination of the airstream in a vertical plane 7.25 feet forward of the elevator hinge line, measured along thrust axis. Vectors show angular deviation of air flow from free-stream direction View looking forward. Propeller operating. Run 30; C_L, 0.820; Ψ, 5°; V/nD, 0.99.

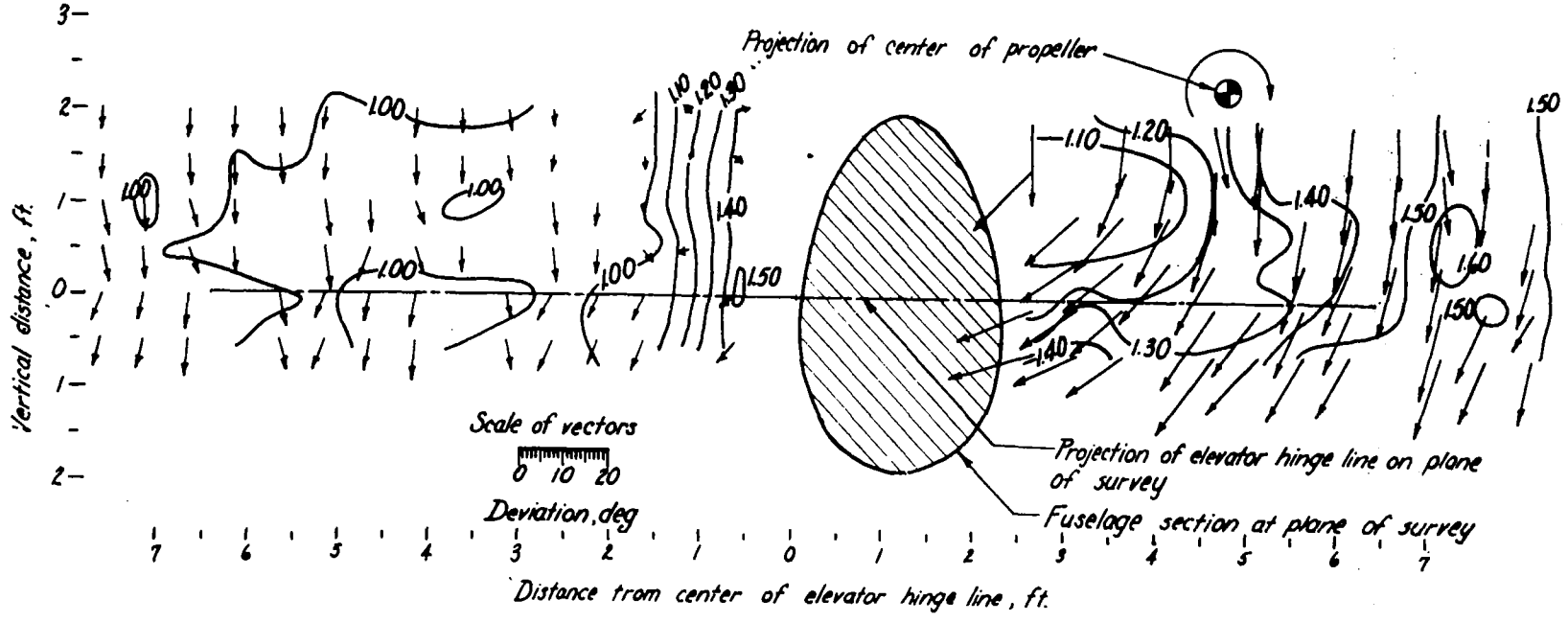

Figure 34.—Dynamic-pressure (q/q_0) contours and inclination of the air stream in a vertical plane 7.25 feet forward of the elevator hinge line, measured along thrust axis. Vectors show angular deviation of air flow from free-stream direction. View looking forward Propeller operating Run 42; C_L, 0.820; Ψ, 10°; V/nD, 0.99.

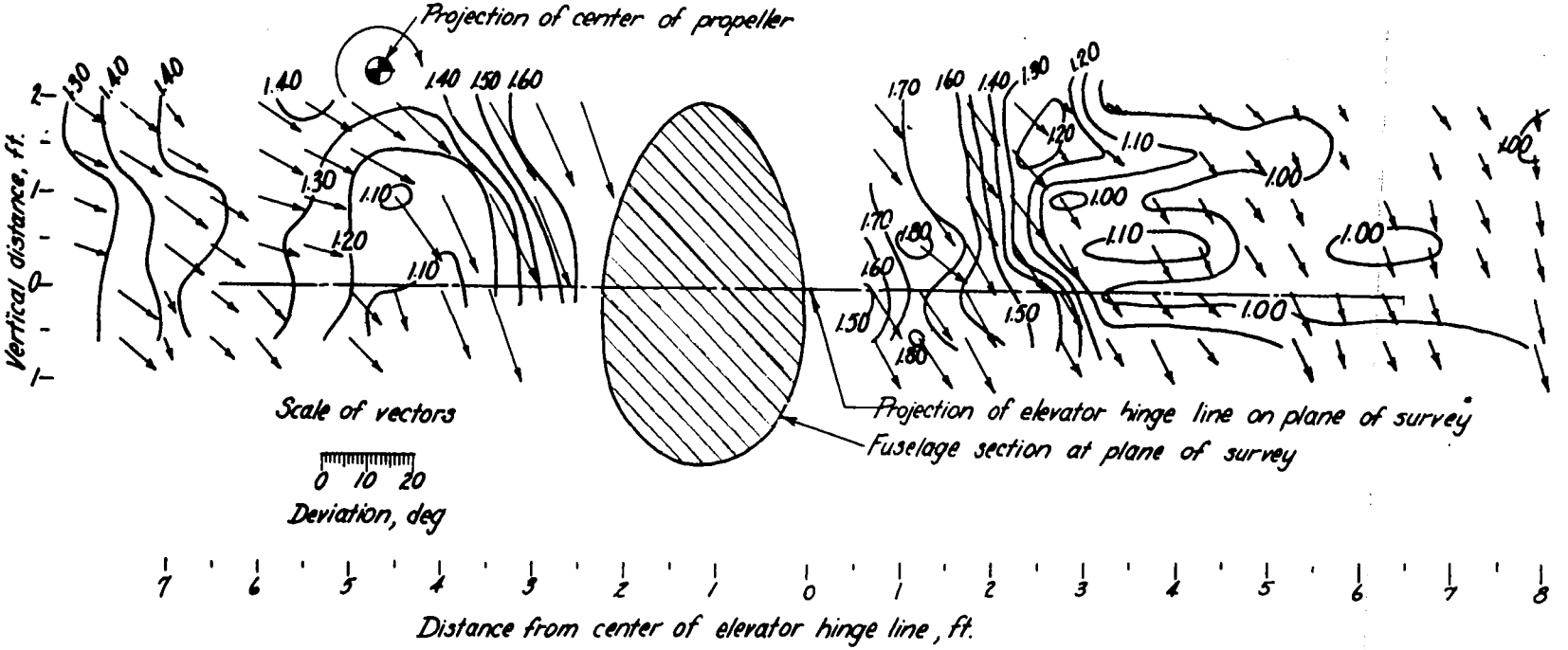

Figure 35.— Dynamic-pressure (q/q_0) contours and inclination of the air stream in a vertical plane 7.25 feet forward of the elevator hinge line, measured along thrust axis. Vectors show angular deviation of air flow from the free-stream direction. View looking forward. Propeller operating. Run 52; C_L, 0.820; Ψ, -10°; V/nD, 0.99.

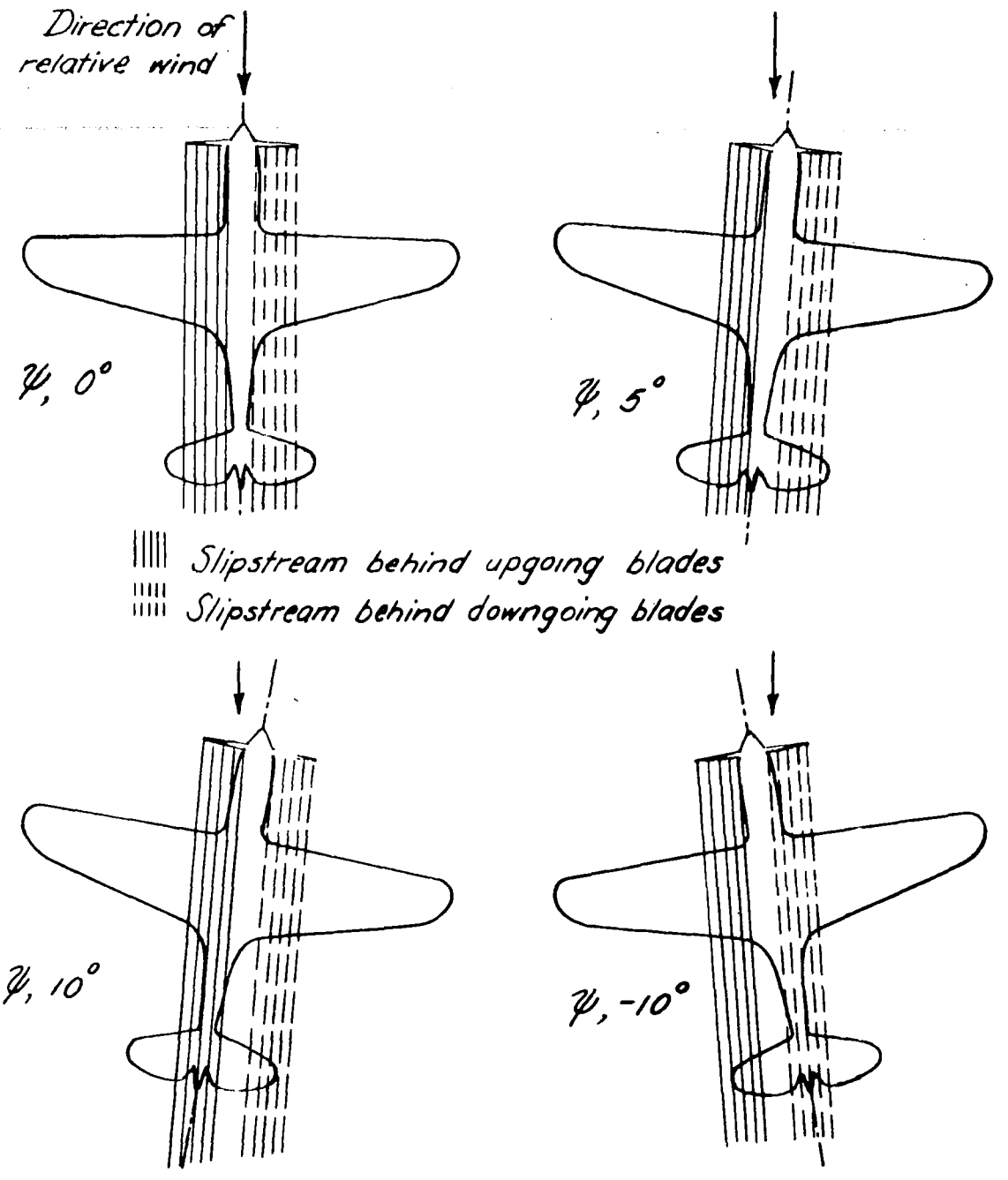

Figure 36.-Sketches showing probable slipstream pattern in yawed flight.

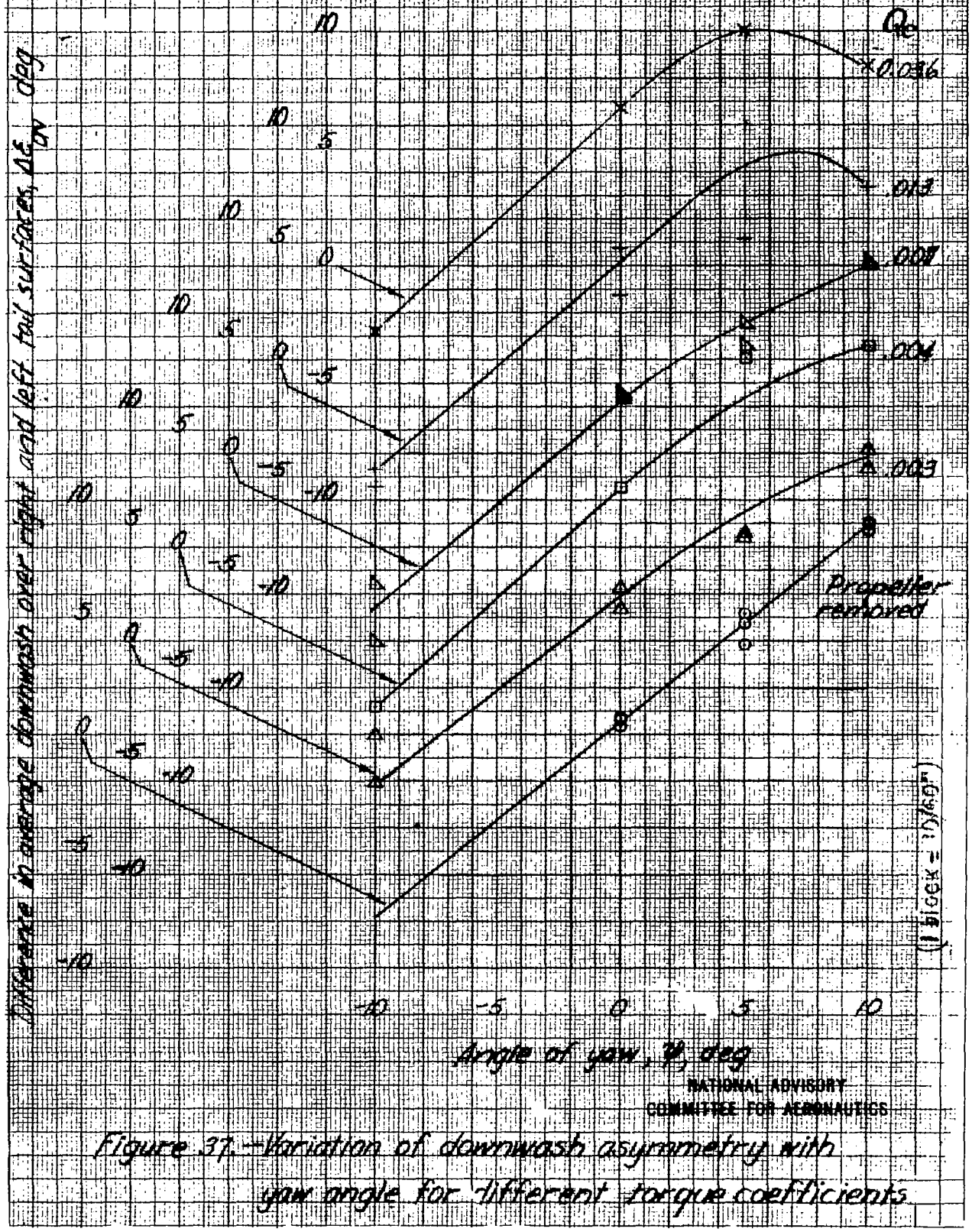

NATIONAL ADVISORY COMMITTEE FOR AERONAUTICS

Figure 37.--Variation of downwash asymmetry with yaw angle for different torque coefficients.

Figure 38. - Variation of $\Delta C_{N_{av}}$ with $\Delta\epsilon_{av}$.

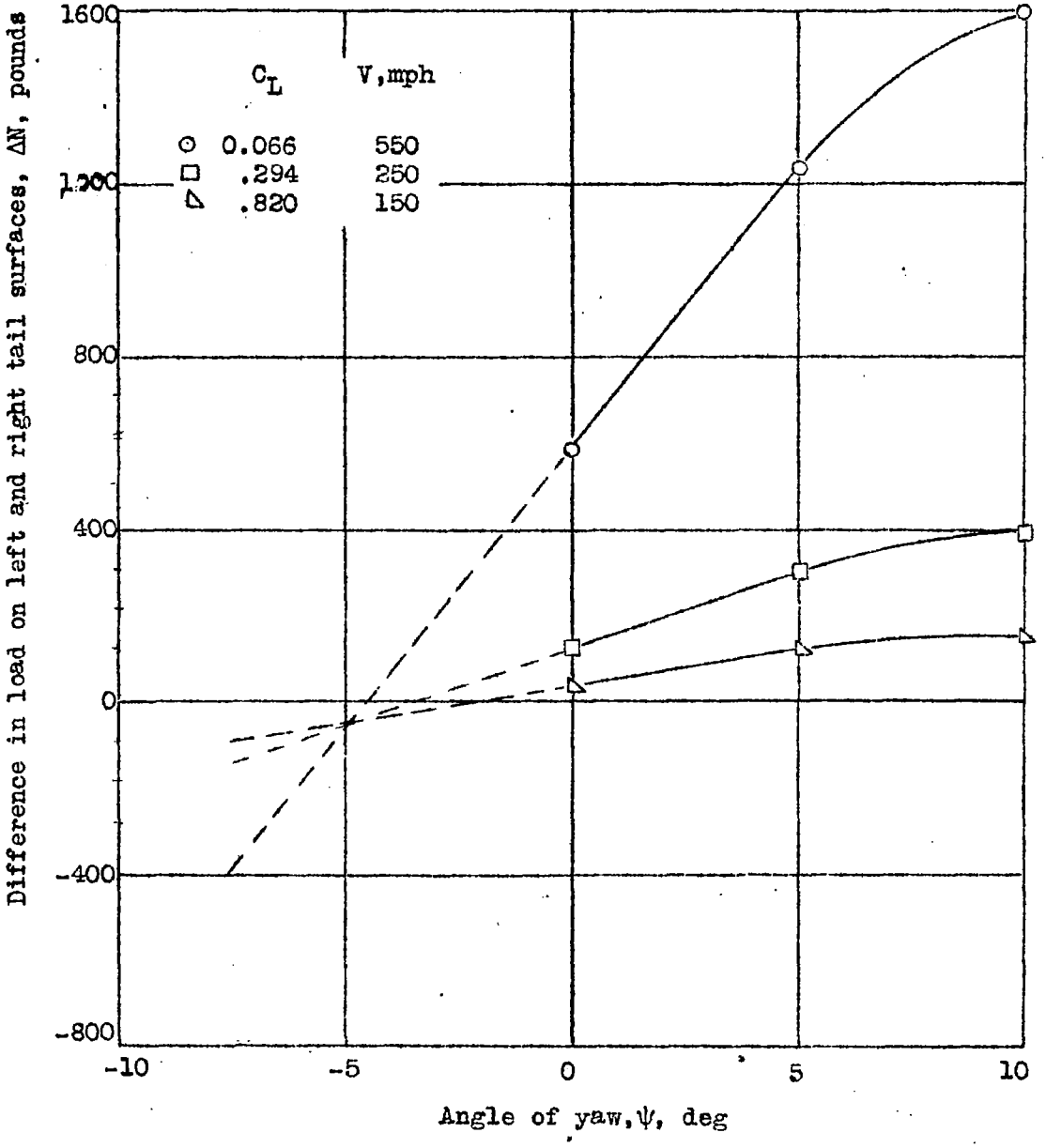

Figure 39.- Load asymmetry measured at several yaw angles for various lift coefficients with the propeller removed. H, 10,000 feet.

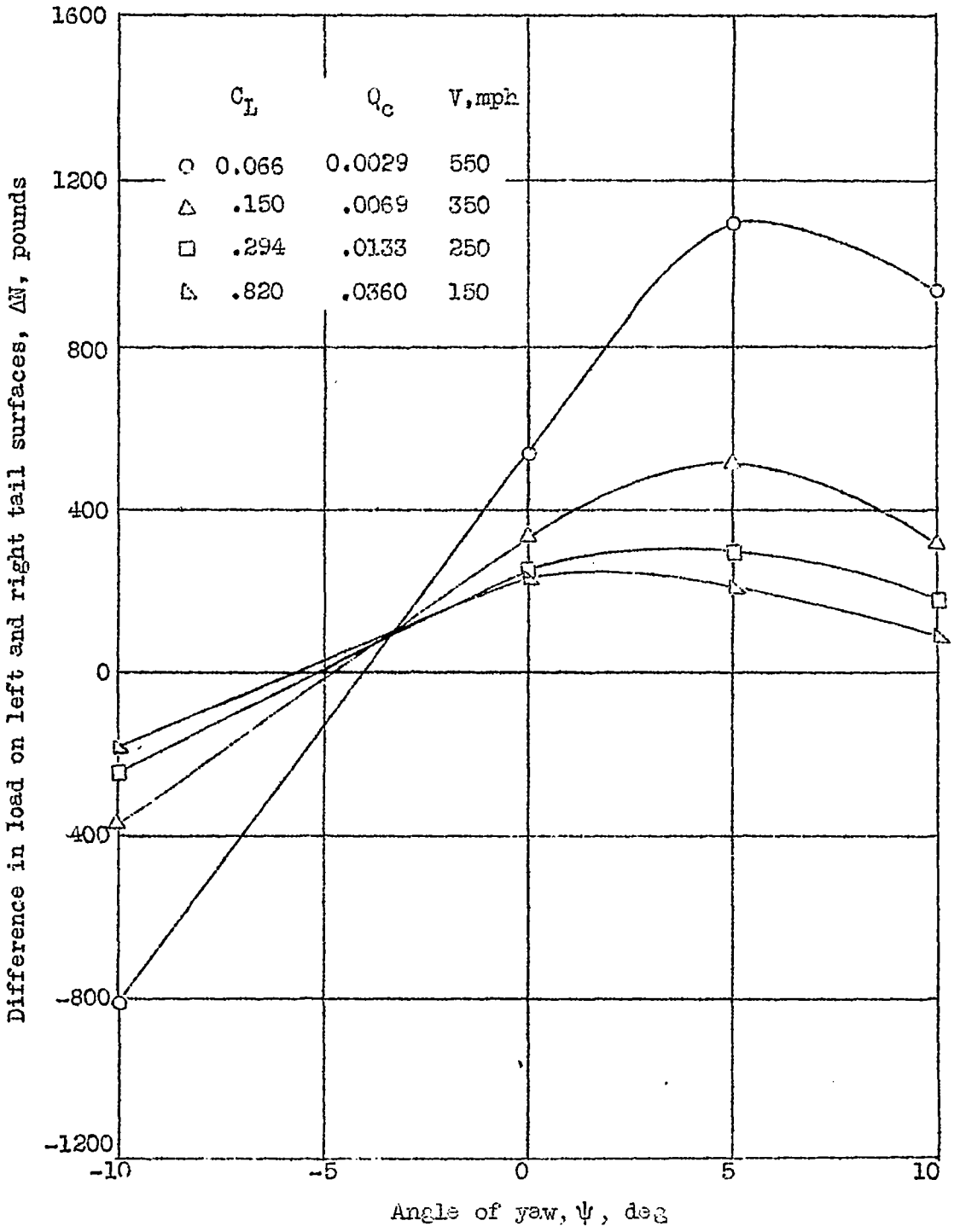

Figure 40 - Load asymmetry measured at several yaw angles for various steady-flight conditions. H, 10,000 feet.

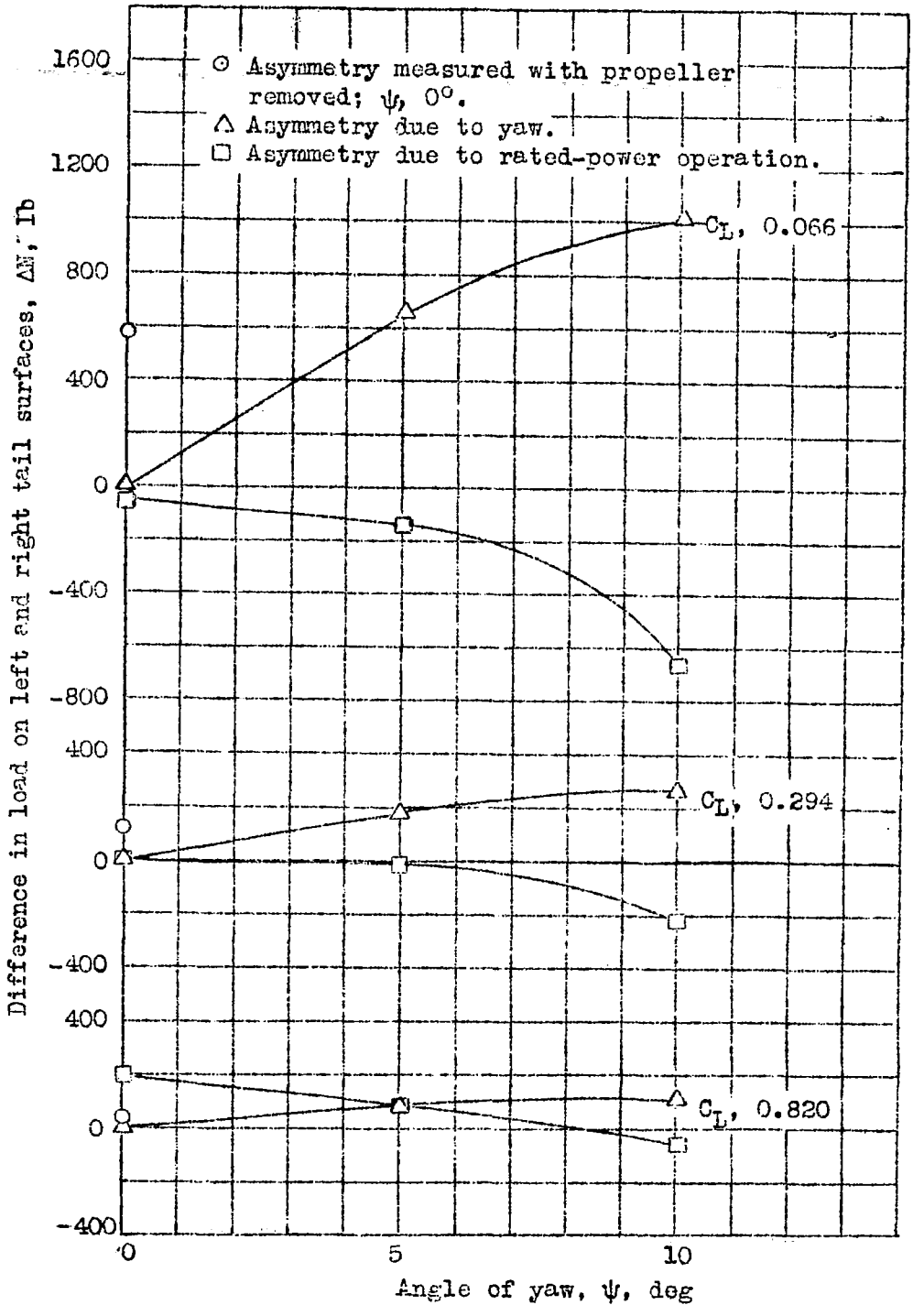

Figure 41.- Effect of yaw and power on the load asymmetry measured for steady-flight conditions.